HHS Public Access

Author manuscript

Cell Microbiol. Author manuscript; available in PMC 2022 April 01.

Published in final edited form as:

Cell Microbiol. 2021 April ; 23(4): e13295. doi:10.1111/cmi.13295.

Cyclophilin 19 secreted in the host cell cytosol by *Trypanosoma cruzi* promotes ROS production required for parasite growth

Gregory Pedroso dos Santos[1], **Fernanda Midori Abukawa**[1], **Normanda Souza-Melo**[1], **Laura Maria Alcântara**[1], **Paula Bittencourt-Cunha**[1], **Carolina Borsoi Moraes**[2], **Bijay Kumar Jha**[3], **Bradford S. McGwire**[3], **Nilmar Silvio Moretti**[1], **Sergio Schenkman**[1,*]

[1]Departamento de Microbiologia, Imunologia e Parasitologia, Escola Paulista de Medicina, Universidade Federal de São Paulo, São Paulo, SP, Brazil

[2]Departamento de Ciências Farmacêuticas, Universidade Federal de São Paulo, Diadema, SP, Brazil

[3]Division of Infectious Diseases/Department of Internal Medicine, The Ohio State University, Columbus, OH, USA

Abstract

Infection by *Trypanosoma cruzi,* the protozoan parasite that causes Chagas disease, depends on reactive oxygen species (ROS), which has been described to induce parasite proliferation in mammalian host cells. It is unknown how the parasite manages to increase host ROS levels. Here, we found that intracellular *T. cruzi* forms release in the host cytosol its major cyclophilin of 19 kDa (*Tc*Cyp19). Parasites depleted of *Tc*Cyp19 by using CRISPR/Cas9 gene replacement proliferate inefficiently and fail to increase ROS, compared to wild type parasites or parasites with restored *Tc*Cyp19 gene expression. Expression of *Tc*Cyp19 in L6 rat myoblast increased ROS levels and restored the proliferation of *Tc*Cyp19 depleted parasites. These events could also be inhibited by cyclosporin A, (a cyclophilin inhibitor), and by polyethylene glycol-linked to antioxidant enzymes. *Tc*Cyp19 was found more concentrated in the membrane leading edges of the host cells in regions that also accumulate phosphorylated $p47^{phox}$, as observed to the endogenous cyclophilin A, suggesting some mechanisms involved with the translocation process of the regulatory subunit $p47^{phox}$ in the activation of the NADPH oxidase enzymatic complex. We concluded that cyclophilin released in the host cell cytosol by *T. cruzi* mediates the increase of ROS, required to boost parasite proliferation in mammalian hosts.

[*]**Correspondence** Sergio Schenkman, R. Pedro de Toledo 669 L6A, São Paulo SP, 04039-032, Brazil, sschenkman@unifesp.br.

AUTHOR CONTRIBUTIONS

Sergio Schenkman, Bradford McGwire, Carolina Borsoi Moraes, obtained funds; Gregory Pedroso dos Santos, Bradford McGwire, Nilmar S. Moretti and Sergio Schenkman planned the experiments; Gregory Pedroso dos Santos, Fernanda M. Abukawa, Bijay K. Jha, Nilmar S. Moretti, Laura Maria Alcantara, Normanda Souza-Melo, Paula Cunha-Bittencourt and Sergio Schenkman performed the experiments; Gregory Pedroso dos Santos and Sergio Schenkman, wrote the first draft of the manuscript; Gregory Pedroso dos Santos, Sergio Schenkman, Bradford McGwire, Nilmar S. Moretti, Bijay Kumar Jha, Normanda Souza-Melo, Fernanda M. Abukawa, Carolina B. Moraes, Laura Maria Alcantara revised and corrected the manuscript.

CONFLICT OF INTEREST

The authors declare no competing interests.

Keywords

Cyclophilin; Protein secretion; *Trypanosoma cruzi*; oxygen radicals; NADPH oxidase

1. INTRODUCTION

Cyclophilins (CyPs), FK-506 binding proteins (FKBPs), and parvulins are immunophilin proteins that act as protein-chaperones (Dornan *et al.*, 2003). CyPs catalyze the cis-trans isomerization of proline residues in polypeptide chains, mediating conformational changes in several proteins (Fischer *et al.*, 2003; Schiene-Fischer, 2014). They constitute a ubiquitous and phylogenetic diversified family, characterized by high evolutionary conservation through prokaryotic and eukaryotic organisms (Wang *et al.*, 2005; Davis *et al.*, 2010).

Mammalian cyclophilin A (CypA) is a cytosolic protein involved in a wide variety of cellular processes, including protein folding, trafficking, cell signaling, and T-cell activation (Nigro *et al.*, 2013). In vascular smooth muscle cells, angiotensin II stimulates CypA secretion by promoting its acetylation and secretion. The secretion occurs through the vesicular pathway, requiring actin remodeling and myosin II activation via RhoA, Cdc42 and Rho-kinase-dependent signaling events (Suzuki *et al.*, 2006; Soe *et al.*, 2014). Secreted CypA binds to its cell surface receptor, CD147, leading to intracellular signaling processes and metalloproteinase 9 activation with increased cell migration capacity (Seizer *et al.*, 2015). Extracellular CypA signaling activates ERK1/2 kinases (Malesevic *et al.*, 2013; Ren *et al.*, 2016; Xue *et al.*, 2018), and causes reactive oxygen species (ROS) production (Satoh *et al.*, 2009) by chaperoning the $p47^{phox}$ subunit to the cell surface to activate NADPH oxidase (NOX2) (Soe *et al.*, 2013). CypA inhibitors prevent several inflammatory processes. For example, these inhibitors improve the outcome of autoimmune myocarditis (Heinzmann *et al.*, 2015), which appears to happen during the chronic phase of Chagas disease (Bonney *et al.*, 2008; Cunha-Neto *et al.*, 2011).

The development of Chagas disease caused by the protozoan parasite *Trypanosoma cruzi* has been associated with increased levels of ROS in the infected tissues and cells (Paiva *et al.*, 2018). ROS enhances proliferation of amastigotes, a parasite form that replicates in the cytosol of infected cells. Several compounds that decrease ROS levels, such as cobalt protoporphyrin (CoPP), catalase (CAT), superoxide dismutase (SOD), the ROS-scavenger phenyl-α-tert-butyl (PBN), resveratrol, tempol, and the SIRT1 agonist SRT1720, prevent parasite proliferation in cultured cells and improve cardiac function in experimental Chagas disease (Wen *et al.*, 2010; Dhiman *et al.*, 2011; Paiva *et al.*, 2012; Wen *et al.*, 2014; Goes *et al.*, 2016; Vilar-Pereira *et al.*, 2016; Dias *et al.*, 2017). Evidence suggests that a moderate oxidative environment is advantageous for *T. cruzi* proliferation. However, it is not completely understood how the parasite induces the generation of ROS during differentiation and infection (Estrada *et al.*, 2018).

Cyclophilin 19 (*Tc*Cyp19) is the major cyclophilin expressed by *T. cruzi* (Potenza *et al.*, 2006). It is secreted by the epimastigote form, which is the stage that proliferates in the insect vector (Kulkarni *et al.*, 2013). It is also found in the secretome of African trypanosomes (Pelle *et al.*, 2002). *Tc*Cyp19 is 71.9% identical to human CypA (Bua *et al.*,

2001), and inhibitors of cyclophilins such as cyclosporin A and its analogs reduce epimastigote proliferation and cellular infection by trypomastigotes (Bua *et al.*, 2004; Carraro *et al.*, 2007; Bua *et al.*, 2008). *Tc*Cyp19 is involved in the oxidant/antioxidant responses of *T. cruzi* (Bustos *et al.*, 2015) and parasites selected by resistance to benznidazole, which acts through oxidative damage, show increased *Tc*Cyp19 expression (Rego *et al.*, 2015).

We hypothesized that *Tc*Cyp19 is secreted by amastigotes proliferating in the host cell cytosol and could functionally mimic CypA during parasite infection. Here, we investigate this possibility by using epitope-tagged *Tc*Cyp19 expressed in the parasites and host cells to verify whether intracellular amastigotes secrete *Tc*Cyp19. We also overexpressed *Tc*Cyp19 either in the parasite, or in the host cell, to determine the extent at which it could modulate the infection and ROS production. In parallel, CRISPR/Cas9 parasite knockdown and addbacks were generated. Our results indicated that secreted *Tc*Cyp19 enhances parasite proliferation rates by inducing increased ROS production by host cells, via a mechanism similar to CypA.

2. EXPERIMENTAL PROCEDURES

2.1. Ethics statement

The procedures used in this work were approved by the “Comite de Ética em Pesquisa da Universidade Federal de São Paulo” under protocol 7164220915. All methods were performed in accordance with the relevant guidelines and regulations approved by the Universidade Federal de São Paulo, which follow Brazilian Animal Practice and Ethics legislation.

2.2. Parasites and Cell Culture

T. cruzi epimastigotes (Y strain) were cultured in liver infusion tryptose (LIT) medium with 10% fetal bovine serum (FBS) at 28ºC, as described (Camargo, 1964). Metacyclic trypomastigotes were generated by *in vitro* differentiation (Contreras *et al.*, 1985). Intracellular amastigotes were obtained through cell lysis 72 hr after the infection of $LLCMK_2$ (Rhesus monkey kidney cells, ATCC CCL-7) cultured in low glucose Dulbecco’s Modified Eagle Medium (DMEM), supplemented with 10% fetal bovine serum (FBS), 59 mg/mL penicillin and 133 mg/mL streptomycin (cDMEM), and kept in a CO_2 incubator at 37 °C. Tissue culture trypomastigotes were harvested from the medium culture supernatant of infected cells, 120 to 144 hours after infection (Abuin *et al.*, 1999). *Rattus norvegicus* skeletal muscle myoblast (L6 CRL-1458) cells were also cultured in cDMEM.

2.3. Western Blot

Extracts were prepared from parasites harvested by centrifugation at 2,000 g for 5 min at 4 °C or L6 cells harvested by centrifugation at 800 g for 5 min at 4 °C and washed once with PBS before lysis. Cell pellets were resuspended in sample buffer and heated at 95 ºC for 5 min. Alternatively, extracts were prepared by lysis in 50 μl of ice-cold lysis buffer [50 mM NaCl, 20 mM Tris-HCl, pH 7.4, containing 1% Triton X100, 1 mM phenylmethanesulfonyl

fluoride (PMSF), and the complete protease inhibitor cocktail, EDTA-free (Roche Life Science)].

The samples were subjected to SDS-PAGE and transferred to nitrocellulose membranes using the semi-dry transfer system (Bio-Rad Laboratories), according to the manufacturer's instructions. After the transfer, the membranes were stained with 0.3% Ponceau S in 3% acetic acid, washed in water, and treated with 5% nonfat milk in PBS containing 0.05% Tween-20 for 60 min. The membranes were incubated for 1 to 12 hr with primary antibodies in PBS containing 0.1% Tween-20. Anti-*Tc*Cyp19 rabbit polyclonal antiserum was obtained by immunization with the recombinant protein cloned in the NdeI and BamHI sites of pET15b (Novagen), expressed in *E. coli* BL21DE3 and purified by Ni^{2+} -agarose affinity chromatography. The serum was used at a dilution of 1:10,000. The following primary antibodies were used at 1:20,000 dilution: anti-Hsp70 (McDowell *et al.*, 1998), anti-*T. cruzi* β-tubulin, anti-eIF5A (Chung *et al.*, 2013) and anti-BiP (Bangs *et al.*, 1993). Anti-influenza virus hemagglutinin (HA.11) (Covance), anti-aldolase (Barbosa Leite *et al.*, 2020) and anti-human CypA (Cell Signaling) were used at 1:5,000, anti-GAPDH (14C10) (Cell Signaling) at 1:10,000 and CypA at 1:5,000. Anti-p47phox (Merck, SAB4502810) were used at 1:500, and anti-,Phospho Ser345 of p47 (PA5–37806) from Thermo-Fisher Scientific at 1:100. Bound antibodies were detected with anti-mouse or -rabbit IgG IRDye 800 and 680 respectively (LI-COR Biosciences), diluted at 1:10.000 in PBS with the Odyssey Fc System.

2.4. Immunofluorescence

Parasites previously washed with PBS were attached to glass slides (Tekdon Inc.) pretreated with 0.01% poly-L-lysine (Sigma-Aldrich) for 5 min. Alternatively, L6 cells were previously seeded in 24 well plates on glass coverslips. Unattached cells were removed, and the slides and coverslips incubated with 4% paraformaldehyde in PBS at room temperature for 20 min, washed in PBS, and permeabilized with 0.1% Triton X100 in PBS for 5 min. The slides and coverslips were then incubated for 20 min with 1% BSA in PBS, followed by 1 hr incubation with primary antibodies diluted in the same buffer. Primary antibodies were diluted as follows: Anti-*Tc*Cyp19 at 1: 5,000, anti-HA at 1:1,000, anti-human CypA at 1:1.000, anti-$p47^{phox}$ at 1:500, anti-P-345 $p47^{phox}$ at 1:100, and anti-green fluorescent protein (A11122-GFP, Thermo-Fisher Scientific) at 1:1,000 dilutions. Bound antibodies were detected with Alexa Fluor 594 or 488 conjugated to goat anti-rabbit or anti-mouse IgG respectively (Thermo-Fisher Scientific) diluted at 1:10,000 in the same buffer of the primary antibodies. Coverslips were mounted in Prolong Gold Antifade Reagent (Thermo-Fisher Scientific) in the presence of 10 μg of DAPI per mL. Images were acquired by a Hamamatsu Orca R2 CCD camera coupled to an Olympus (BX-61) microscope equipped with a x100 plan Apo-oil objective (NA 1.4). Acquisitions were at every 0.2 μm for each set of excitation/emission filters. Blind deconvolution was performed by employing the AutoQuant X2.2 software (Media Cybernetics).

Alternatively, immunofluorescence was performed with infected mammalian cells seeded on round glass coverslips. The cells were fixed with 0.2% glutaraldehyde in PBS, and incubated with a quench solution (1% sodium borohydride, 1% disodium hydrogen phosphate monohydrate solution) (Bangs *et al.*, 1993). The following steps were performed as

described above. The images were acquired by Leica TCS SP5 confocal system (Leica Microsystems, Wetzlar, Germany) using a 100X (NA 1:44) oil immersion objective, and processed with AutoQuant X2.2 software (Media Cybernetics). The super-resolution microscopy images were acquired by a Leica TCS STED equipped with an inverted microscope (DMI 6000, Leica) and a 100X STED objective (HCX PLAPO100X, 1.4 oil STED, Leica).

2.5. Trypomastigote and amastigote secretion assays

To analyze the *Tc*Cyp19 secretion by tissue culture trypomastigotes (5×10^7/mL), the parasites were placed in 1.5 mL tubes with 1 mL of cDMEM containing 20 mM Hepes and adjusted to pH 7.4 by the addition of 1 N NaOH, or 1 N HCL to pH 5.0, and kept for 5 hr at 37 °C in a CO_2 incubator. Parasites were then collected by centrifugation (5 min at 2000 g), the supernatant was discarded, and the parasite resuspended in 0.3 mL of cDMEM at pH 7.4 and maintained at 37 °C for another 19 hr After this last incubation, the parasites were centrifuged, and the supernatant or parasites lysed with SDS-PAGE sample buffer. At each step, the amount and morphology of parasites were quantified by microscopic analysis.

To detect secretion by intracellular amastigotes, L6 cells plated in a T-150 cell culture flask were infected with fresh tissue culture derived trypomastigotes at MOI of 20:1. After 12 hr of infection, cells were washed with PBS and incubated for 108 hours. The cells were washed with warm PBS (37°C) and removed from the bottle using a cell scraper. The cell suspension was centrifuged for 5 minutes at 200 g and resuspended in 1 mL of PBS solution containing protease inhibitors (200 ng aprotinin, 20 μg pepstatin and 2 μg leupeptin nad 0.1 mM PMSF) and lysed manually in a 5 mL Potter-Elvehjem glass homogenizer with a Teflon pistil. After lysis, confirmed by microscopic examination, the cell debris was removed by centrifugation at 200 g for 10 min and the supernatant with parasites was submitted to 3 steps of centrifugation at 2,000 g for 5 min and the final supernatant and the pellet containing parasites incubated with SDS-PAGE sample buffer.

2.6. Generation of genetically modified parasites and mammalian cells

The *T. cruzi* gene of *Tc*Cyp19 (TcCLB.506925.300, http://tritrypdb.org), was amplified by PCR with the genomic DNA of the Y strain as template, using the oligonucleotides *Tc*Cyp19BamHIfow and *Tc*Cyp19HAXbaIrev (Table S1). The amplified fragment was cloned in the pGEM-T Easy vector plasmid (Promega). The constructions were confirmed by restriction analysis and sequencing. The fragment containing the *Tc*Cyp19 gene was removed by cleavage with the enzymes BamHI and XbaI, and inserted into the plasmid vector p33 (Ramirez *et al.*, 2000) and the plasmid vector pCDNA 4TO (Thermo-Fisher Scientific) previously digested with the same restriction enzymes. The sequence of the green fluorescent protein (GFP) was derived from plasmid pXG-GFP and inserted into the pCDNA 4TO plasmid as described (de Paulo Martins *et al.*, 2010).

T. cruzi transfections were performed using epimastigote in the exponential growth phase, previously washed and resuspended to 1×10^7 parasites in 100 μl of electroporation buffer (137 mM NaCl, 5 mM KCl, 5.5 mM Na_2HPO_4, 0.77 mM glucose and 21 mM Hepes, pH 7.0) and pulsed with the Amaxa Nucleofector (Lonza) using the X-014 program. Cells were

then diluted in LIT culture medium and selection performed with 0.2 to 0.5 mg/mL G418 (Thermo-Fisher Scientific). L6 cells containing the pCDNA 6TR were transfected using lipofectamine LTX plus reagent by the recommended procedures (Thermo Fisher Scientific), selected with 150 μg/mL zeocin (Invitrogen) and posteriorly cloned by limiting dilution. We observed that expression of the cloned genes occurred independently of the addition of tetracycline, and therefore the experiments were carried out in the absence of this antibiotic.

For generation of CRISPR/Cas9 modifications in *T. cruzi*, we used the recombinant *S. aureus* Cas9 (SaCas9) cloned in the plasmid pET32 EK-Lic (Novagen) provided by Lia Carolina Soares Medeiros (ICC, Fiocruz, Brazil), prepared as described (Soares Medeiros *et al.*, 2017). The single guide RNA sequences (sgRNA) and the donor DNA strands, were developed using the tools available at http://grna.ctegd.uga.edu as described (Peng *et al.*, 2015), using the target sequence of 21 bp that precedes a PAM NNGRRT site. PCRs were performed to generate the sgRNA for SaCas9 system and the DNA donor strands. Oligonucleotides *Tc*Cyp19_199_sgRNA1 and REVSaCas9_scaffold_WDR were used for amplification of the sgRNA from the plasmid pTZ57 (Ran *et al.*, 2015), also provided by Lia Carolina Soares Medeiros. To amplify the DNA donor with blasticidin resistance mark we employed oligonucleotides FOW5'UTR_sgRNA1_*Tc*Cyp19 and REVpos-PAM_sgRNA1_*Tc*Cyp19 and the plasmid pTrex-b-NLS-hSpCas9 (Addgene plasmid # 62543).

The sgRNA was prepared by *in vitro* transcription using the MEGAShortscript transcription kit (Thermo Fisher Scientific) (Lander *et al.*, 2015). SgRNA products and DNA donor fragments were purified by ethanol precipitation by standard procedures. The sgRNAs were prepared immediately before transfections. Annealing of sgRNAs was carried out by heating RNA at 90 °C for 5 min and cooling slowly in ice, followed by adding equimolar amounts of SaCas9 (11 ratio). The samples were then incubated at room temperature for 10 to 15 min. Approximately 40 μg of DNA donor strand was used in the transfection as described above, except that the selection was in medium containing 0.1 mg/mL blasticidin. Detection of the correct insertion of the blasticidin marker was performed with the total DNA extracted from parasites using standard procedures and PCR using primers P1 and P2, or P3/P2 followed by electrophoresis in agarose gels and ethidium bromide staining.

2.7. Parasite infection

The different L6 cell lineages (wild type, GFP and *Tc*CyP19-HA), previously seeded at 800 cells per well in a 384-well plate containing 40 μL of cDMEM, were infected with an MOI 20:1 using the different tissue culture derived trypomastigotes lineages (wild type, GFP and *Tc*Cyp19-HA) for 5 hr, kept in a CO_2 incubator at 37ºC. The media were removed, the wells washed with PBS and fresh medium added. The parasite multiplication was followed from 24 to 96 h. The medium was removed every day and cells were fixed with 4% paraformaldehyde in PBS and stained with Draq5 (Biostatus). The plates were scanned using a High Content Imaging System In Cell Analyzer 2200 (GE) at 20X magnification and the acquired images analyzed by using In-Cell Investigator Software 1.6 (GE). Five images of each well were acquired and analyzed to determine the infection and proliferation ratios.

Three different sets of infections were performed. Non-infected cells were used as negative controls.

Alternatively, to analyze the infection of the parasites *Tc*Cyp19 depleted and *Tc*Cyp19-HA add-backs, 1.5×10^4 L6 cells were seeded in 24 well plates previously prepared with glass coverslips and maintained in 500 μL of cDMEM at 37°C. After 24 hr, the media were removed, and the cells infected with trypomastigotes (MOI of 20:1) in 0.5 mL for 5 hr in a CO_2 incubator at 37ºC. At the indicated times, cells were washed with PBS, the coverslips were collected, fixed with 4% paraformaldehyde in PBS and stained with Hoechst 33342 (Sigma-Aldrich) to label the cell and parasite nucleus. When indicated, superoxide dismutase–polyethylene glycol, catalase−polyethylene glycol, or cyclosporin A (C1832–5MG), all from Sigma-Aldrich, were added at 48 hr post-infection. Parasite numbers and proliferation rates were calculated by identifying infected cells and counting the nucleus of the parasites. Each analysis was performed in triplicate experiments by counting 100 infected cells on acquired images using a Hamamatsu Orca R2 CCD camera coupled with an Olympus BX-61 microscope.

2.8. Reactive oxygen species measurements

L6 cells were seeded to 24-well plates on glass coverslips and kept in a CO_2 incubator at 37ºC. The next day, the cells were treated according to the protocol of the CellROX Deep Red kit (Thermo Fisher Scientific). Images were acquired using a Hamamatsu Orca R2 CCD camera coupled with an Olympus (BX-61) microscope. Alternatively, L6 cells were plated in a black 96-well plate with a transparent bottom and kept in a CO_2 incubator at 37ºC for 24 h. The cells were then incubated separately with 25 μM of CM-H_2DCFDA (Thermo Fisher Scientific) and with a solution of 1:3,000 of Hoechst 33342, both diluted in Hank's balanced salt solution buffer. The plate was maintained in the CO_2 incubator at 37ºC for 45 min. After the incubation period, the wells were washed 3 times with 100 μL of HBSS and then immediately read in a SpectraMax M3 plate reader (Molecular Devices) with Ex/Em: 485/535 nm for CM-H_2DCFDA and Ex/Ex: 361/486 nm for the Hoechst dye. The same procedure was carried out to analyze ROS levels in cells treated with 15 μM cyclosporine and/or infected with tissue culture derived trypomastigotes.

2.9. Cell migration and growth assays

The cell migration assays were performed in 24-well plates by scraping the monolayer. After washes in PBS, the cells were then incubated with 5 μg/mL of aphidicolin (Merck-Millipore) and migration followed with an Axio observer Z1 Zeiss microscope by taking images every 6 hr for 48 h. Migration was quantified by measuring the initial and empty area using Fiji ImageJ (v. 2.0) software. Cell growth was quantified by plating 750 cells in 96 well plates in cDMEM. After growth, the cells were fixed with 4% paraformaldehyde in PBS for 15 min and stained with Draq5. The number of cells was estimated using the InCell Investigator in 7 fields of each well.

2.10. Sequence, statistical and deconvolution analyses

The protein sequences were analyzed using Geneious 11.1.15 software. Graphical and statistical analyses were performed using Prism 7 (GraphPad) software Version 6.01.

Colocalization analysis was performed either using the colocalization test in the Fiji package of ImageJ or by using the plugin in the software Autoquant 2.2. In this later case a threshold was applied to consider the signals above 25% of the total gray level for the images in one section after blind deconvolution.

3. RESULTS

3.1. *Tc*Cyp19 is similar to CypA and expressed in all *T. cruzi* stages

The alignment of *Tc*Cyp19 and CypA indicates that 71.9% of the amino acid residues along the protein chain are conserved and some post-translational modified residues found in mammals appear conserved in the *T. cruzi* (Fig. 1A). For instance, the lysines 82 and 125, in which acetylation is relevant for CypA secretion and production of ROS by vascular smooth muscle cells and endothelial cells in the presence of angiotensin II (Soe *et al.*, 2013; Soe *et al.*, 2014), are present in *T. cruzi* as lysines 92 and 138. Also, a proteomic analysis of acetylated lysine in *T. cruzi* epimastigotes identified two acetylated lysines at positions 4 and 54 (Moretti *et al.*, 2017), with the latter also acetylated in CypA. Are also conserved the key residues involved in the active site and the residues described to interact with CsA, which is reported to affect the *T. cruzi* cyclophilins (Carraro *et al.*, 2007; Carraro *et al.*, 2016). The major difference of CypA is in the first ten amino acids of *Tc*Cyp19, also present in all related cyclophilins of trypanosomatids.

*Tc*Cyp19 was found expressed at higher level in epimastigotes and detected in similar amounts in metacyclic-trypomastigotes, intracellular amastigotes and trypomastigotes obtained from tissue culture cells when compared to the Bip protein, an endoplasmic reticulum chaperone (Fig. 1B and C). *Tc*Cyp19 was found distributed in all cytosol of the different parasite stages, although a more punctate localization was observed in the trypomastigote stages (Fig. 1C).

3.2. Generation of *T. cruzi* expressing tagged *Tc*Cyp19 protein

As antibodies produced against the parasite cyclophilin cross-reacted with CypA due to their close similarity, we generated a *T. cruzi* cell line that constitutively expressed *Tc*Cyp19 protein fused to the hemagglutinin (HA) epitope at C-terminal (*Tc*Cyp19-HA) to distinguish the parasite and mammalian proteins. Epimastigotes were transfected with the p33 plasmid with the *TcCyp19-HA* gene and selected for G418 resistance. Western blotting of wildtype and transfects indicates that in both trypomastigotes and intracellular amastigotes, *Tc*Cyp19-HA was expressed and migrates more slowly in the SDS-PAGE due to the presence of the HA epitope (Fig. 2A). Furthermore, the *Tc*CyP19-HA protein (20 kDa) was recognized by anti-*Tc*Cyp19 antibodies, while the endogenous protein (19 kDa) was not detected using the anti-HA antibody. Quantitative analysis indicated that the *Tc*Cyp19-HA was less expressed in both trypomastigotes and amastigotes when compared with the endogenous protein. Nevertheless, the total amount of *Tc*Cyp19 (endogenous plus the tagged version) was increased in intracellular amastigotes (Fig. 2B). In addition, these levels were higher in amastigotes relative to tubulin, which is expected, as trypomastigotes contain the flagella and an elongated body sustained by subpellicular microtubules. Immunofluorescence

analysis also showed that the exogenous *Tc*Cyp19 was expressed in the cytosol of both amastigotes and trypomastigotes and co-localize with the endogenous protein (Fig. 2C).

3.3. Intracellular amastigotes secrete *Tc*Cyp19 into the host cell cytosol

To evaluate whether *Tc*Cyp19 is secreted by intracellular amastigotes into the host cell cytosol, we infected L6 myoblasts with parasites expressing the *Tc*Cyp19-HA and analyzed them from 24 to 120 hr post-infection (PI) (Fig. 3). Uninfected cells showed a low degree of staining with anti-*Tc*Cyp19 antibodies due to the expected cross-reaction with CypA, whereas no labeling was detected with anti-HA antibodies. In contrast, the anti-HA recognized intracellular amastigotes in recently infected cells, showing an intense cytosolic pattern. At 48 hr PI the *Tc*Cyp19-HA could be detected outside the amastigotes and within the host cell cytoplasm. A few parasites detected by the nuclear staining were not labeled by HA, possibly because of their loss of plasmid, or their inability to express the protein (see arrowheads in merged images). The secretion of *Tc*Cyp19-HA increased and could be better visualized between 72 and 96 hr PI due to increased extent of *Tc*Cyp19-HA secretion and accumulation, filling the host cell cytosol, which interestingly appeared more concentrated at some points close to the membrane edge, as indicated by the arrows (Fig. 3).

Confocal immunofluorescence microscopy of cells 120 hr PI clearly indicated that *Tc*CyP19-HA secretion was present in the host cell cytosol, with accumulation in some areas close to the edge of the cell membrane (Fig. 3A). To exclude the possibility that the labeling corresponded to a fragment of *Tc*Cyp19, or just the HA sequence, a Western blot analysis was performed with extracts of the cytosolic fraction of infected L6 cells (Fig. 3B). *Tc*Cyp19-HA was detected in the cytoplasmic fractions of infected L6 cells while we did not detect eukaryotic translation initiation factor 5A (eIF5A), an abundant protein in the *T. cruzi* cytosol (Chung *et al.*, 2013). This indicates that the presence of *Tc*Cyp19 was not due to amastigote lysis during extraction and did not corresponded to its degradation products. Mammalian glyceraldehyde 3-phosphate dehydrogenase (GAPDH) was present in the fractions, indicating the presence of host cell cytosol elements. Taken together these data confirm the presence of *Tc*Cyp19-HA in the host cell cytosol from 48 hr, which gradually increased up to 120 hr post-infection.

3.4. *Tc*Cyp19-HA expression in L6 myoblast cells increases intracellular parasite multiplication

Next, we generated stable L6 cells expressing HA-tagged *T. cruzi* cyclophilin 19 (L6-Cyp19-HA). Immunofluorescence analysis using anti-HA antibody indicated the expression of *Tc*Cyp19-HA in the cytosol of non-infected L6 cells, with similar distribution to the endogenous CypA, but different to the distribution of GFP (Fig. 4A). In addition, both appeared concentrated in various regions of the cell membrane, resembling the localization of *Tc*Cyp19-HA secreted by amastigotes late in infection (Figs. 3). The expression of *Tc*Cyp19-HA was confirmed by Western blotting of L6-Cyp19-HA cells using anti-*Tc*Cyp19 and HA antibodies (Fig. 4B). The exogenous protein with migration of 20 kDa was weakly recognized by the anti-CypA antibody, which was present in similar amounts in control and *Tc*Cyp19 expressing cells, as a 17 kDa band. The data indicate that *Tc*Cyp19-

HA derived from amastigotes secretion or produced by L6-Cyp19, cells displayed similar localization when compared to CypA in control L6 cells.

We then analyzed the effect of *Tc*Cyp19 produced in both cellular models on the modulation of *T. cruzi* infection and multiplication. Control and L6 cells expressing GFP or Cyp19 were infected with WT trypomastigotes. In parallel, WT L6 cells were infected with WT trypomastigotes or those expressing GFP or *Tc*Cyp19-HA. We used WT cells and those expressing GFP as controls, to exclude the possibility that exogenous protein affected infection and/or parasite growth.

The total number of amastigotes (Figs. 5A and C), which reflects the infectivity and the number of amastigotes in infected cells (Figs. 5B and D), which in turn denotes the parasite proliferative capacity, indicated no significant differences within 24 hr PI in both groups, suggesting that the same proportion of trypomastigotes was able to infect all host cells. After 72 hr, the number of amastigotes were larger, both in cells and in parasites that expressed *Tc*Cyp19 compared to non-transfected or GFP expressing cells. The differences were even greater at 96 hr post infection. These results indicated that increased expression of *Tc*Cyp19, whether parasite- or host cell-derived, favors intracellular amastigote multiplication.

3.5. *Tc*Cyp19-HA expression increases ROS levels in L6 cells

As *T. cruzi* intracellular growth at the later stages of infections is related to the redox state within host cells (Dias *et al.*, 2017; Paiva *et al.*, 2018), we hypothesized that the increased amastigote proliferation in our system was related to increased ROS levels. Hence, we performed microscopic fluorescence analysis to assess the basal levels of ROS production in L6-Cyp19-HA cells using the cell membrane permeable probe CellROX® Deep Red. This probe emits fluorescence upon its oxidation. We therefore, observed more fluorescence when comparing *Tc*Cyp19-expressing L6 cells with controls expressing GFP or L6 cells alone (Fig. 6A). For quantitative analysis we used CM-H2DCFDA probe, which confirmed the increased basal ROS production in L6-*Tc*Cyp19-HA cells (Fig. 6B). To evaluate the contribution of *Tc*Cyp19 on ROS production further, cells were pre-treated with cyclosporine A (CsA), a well-known inhibitor of cyclophilin function. A significant reduction in the ROS was observed compared to control cells (Fig. 6B). As ROS production increases in host cells during infection (Dias *et al.*, 2017), we measured ROS production generated in different L6 cells infected with wild type parasites, or those expressing *Tc*Cyp19-HA or GFP. As seen in Fig. 6C, the increase in the ROS levels was more pronounced from 72 hr post-infection in parasites expressing the *Tc*Cyp19-HA.

We also examined whether other properties of L6-cells containing *Tc*Cyp19 that could interfere with parasite development, as CypA modulates several intracellular events (Xue *et al.*, 2018). *Tc*Cyp19-HA containing cells showed an increased wound-healing capacity (Fig. S1A and B) unrelated to augmented cell proliferation (Fig. S1C). These results are compatible with an increase in ROS in the *Tc*Cyp19-HA expressing cells known to increase cell migration (Nigro *et al.*, 2011).

3.6. Depletion of *Tc*Cyp19 decreases late amastigote multiplication that is restored by expression of *Tc*Cyp19 in cells

To validate that *Tc*Cyp19 expression can modulate *T. cruzi* multiplication inside host cells, we generated parasites with diminished *Tc*Cyp19. For this, we utilized the clustered regularly interspaced short palindromic repeats–CRISPR-associated protein 9 (CRISPR-Cas9) methodology to insert a blasticidin (BSD) resistance marker at the beginning of *Tc*Cyp19 ORF (Fig. 7A). After two rounds of transfection and 30 days of drug selection, we obtained a population of epimastigotes with more than 95% decrease in *Tc*Cyp19 expression and confirmed the *Tc*Cyp19 gene deletion and BSD gene insertion (Fig. 7B). A Western blotting showed some *Tc*Cyp19 remaining after a first round of transfection (1p) and almost full decrease after a second transfection (2p, Fig. 7C). The line was termed KD. M We then generated an add-back control (AB) lineage using the *TcCyp19* deficient lineage through the insertion of plasmid p33*Tc*Cyp19-HA. The KD and AB epimastigotes were differentiated *in vitro* to produce initially metacyclic-trypomastigotes, able to infect cells and generate tissue-culture trypomastigotes. The *Tc*Cyp19 in KD trypomastigotes population showed some residual *Tc*Cyp19 expression (~15–20%) (Fig. 7D and F). Moreover, we found that endogenous *Tc*Cyp19 expression of the KD trypomastigotes increased after few passages in mammalian cells. As we started from a non-cloned population, we surmise that this probably occurred because of the reduced fitness of KD parasites and the selection of few heterozygotes containing residual intact *Tc*Cyp19 gene(s). Nevertheless, we noticed a major reduction of *Tc*Cyp19 in trypomastigotes by immunofluorescence staining and not few fluorescent parasites (Fig. S2), indicating that an extra copy of the gene could have remained in all population. In fact, after a few passages in culture the wild type phenotype was regained, indicating a strong pressure to keep the protein. We also tried without success to obtain clones fully depleted of *Tc*Cyp19 gene, further indicating the requirement of this protein for normal growth. Nevertheless, the obtained AB trypomastigotes showed the full reestablishment of *Tc*Cyp19 expression with *Tc*Cyp19-HA, as shown by immunofluorescence experiments (Fig. S2), which allow us to further evaluate the role of *Tc*Cyp*19* depletion in the parasite infection and proliferation.

We then used these three parasite lines to compare the ROS levels induced by infection of host cells. We observed a clear increase in the ROS production in host cells infected with wild type parasites than those infected with KD parasites (Fig 7G). The ROS production was fully restored in cells infected by the add-back line. This suggests that *Tc*Cyp19 could modulate the ROS production during infection.

3.7. *Tc*Cyp19 increases the multiplication rates through ROS modulation

To evaluate the role of *Tc*Cyp19 in *T. cruzi* multiplication more precisely, we compared the intracellular growth of control, KD and AB parasite lines upon infection of control L6 and L6-CyP19 cells. We found no significant difference in the establishment of infection observed at 24 hr in all cases (Fig. 8A and B). The initial proliferation observed after the first round of amastigotes generation was also independent of the presence of *Tc*Cyp19 in our system. Conversely, at 72 and 96 hr PI, KD parasites showed decreased number of amastigotes per infected L6 cells, indicating reduced proliferation, which could be reverted in the AB parasites (Fig. 8C). More important, the reduced replication of KD parasites

compared to WT and AB parasites in L6 cells was also restored in L6-CyP19 cells (Fig. 8D), indicating that the effect of *Tc*Cyp19 deficiency in the parasites could be reverted by expressing *Tc*Cyp19 in the host cells. This suggests that secreted *Tc*Cyp19, rather than intracellular protein within parasites, was responsible for their diminished growth.

To analyze the role of *Tc*Cyp19 further and compare its influence on ROS production, infected cells were incubated at 48 hr PI with 20 μM of CsA, 25 units of polyethylene-glycol catalase (CAT-PEG) or 20 units of polyethylene-glycol superoxide dismutase (SOD-PEG), which enter cells and were found to display a robust effect in the reduction of parasite multiplication (Bua *et al.*, 2004; Goes *et al.*, 2016; Dias *et al.*, 2017). These treatments all showed a similar effect in amastigote multiplication, reducing the number of amastigotes, as found for the infection by the KD parasites. Moreover, the treatments with antioxidants and CsA reduced parasite proliferation in all infections, indicating a clear relationship between the presence of *Tc*Cyp19 in host cells, parasite multiplication and ROS production.

3.8. *Tc*Cyp19-HA and p47^{phox} of Nox2 are concentrated in the edges of L6 cells

In vascular smooth muscle cells under angiotensin II stimuli, CypA acts in the translocation of the p47^{phox} subunit through the cell cytoskeleton to the caveolae regions, where p47^{phox} activates the multi-component enzymatic complex, NADPH oxidase (NOX2), which consequently increases ROS production (Soe *et al.*, 2013). Using immunofluorescence analysis, we found accumulation and co-localization of CypA and p47^{phox} in the cell edges associated with microfilaments stained by phalloidin (Fig. 9A). Similar localization was obtained by comparing the labeling of *Tc*Cyp19-HA and p47^{phox,} and the cell actin filaments in the L6-CyP19 cells (Fig. 9B). Analysis of several images show some degree of colocalization between *Tc*Cyp19-HA and p47^{phox}, with a volume colocalization of 40% and a Pearson's' correlation coefficient of 0.6 when considering the full image (Fig. S3). Immunofluorescence were also subjected to STED-confocal super-resolution microscopy, which allowed the localization of these proteins in L6-CyP19-HA cells. Unfortunately, the signals of p47^{phox} was not sufficiently strong for the STED analysis, so the corresponding STED of *Tc*Cyp19-HA was matched to the confocalized image of p47^{phox}. As shown in Fig, 9C *Tc*Cyp19-HA labels throughout the cell cytosol and near membrane edges in regions that also contained p47^{phox} . In addition, highly magnified images showed labeling of p47^{phox} aligned by striae associated with *Tc*Cyp19-HA (bottom panels in Fig. 7C), suggesting that it could be involved in the activation of NOX2 in particular regions of the cell.

To further verify the possible role of *Tc*Cyp19 in the Nox2 activation, we performed immunofluorescence analysis of wild type and *Tc*Cyp19-HA cells using both anti-HA and antibodies to the phosphorylated p47^{phox} at Ser 345. A clear colocalization was verified, mainly at the cell migrating edges (see arrows) when considering single Z-sections (Fig. S4A). Interestingly, when we incubated the cells with CsA, the colocalization decreased (Fig. S4B) and most striking was that phosphorylated p47^{phox} was found around the nucleus as indicated by arrowheads. Moreover, we remarked an increased p47 phosphorylation, which was also reduced by incubation with CsA (Fig. S4C).

4. DISCUSSION

Here we show that *T. cruzi* cyclophilin 19 is secreted in the cytosol of infected host cells and enhances parasite multiplication by increasing ROS production, previously found to be critical for this parasite development in cells and tissues (Paiva *et al.*, 2014; Paiva *et al.*, 2018). Our results also suggest that such an increase in the ROS levels might involve the transport of the $p47^{Phox}$ by *Tc*Cyp19, which is analogous to what has been shown for CypA (Soe *et al.*, 2013; Meijles *et al.*, 2014). We propose that one of the roles of secreted parasite cyclophilin is the modulation of the intracellular environment within host cells to allow efficient parasite multiplication.

All *T. cruzi* stages express Tc*Cyp19* in the parasite cytosol. We have previously demonstrated that *Tc*Cyp19 is secreted by epimastigotes and may have a role in parasite survival and growth in the insect vector (Kulkarni *et al.*, 2013). It is possible that *Tc*Cyp19 secretion initiates during the amastigogeneses within parasitophorous vacuoles, as we observed that trypomastigotes pulsed in DMEM at pH 5.0 for 5 hr differentiate, as shown before (Tomlinson *et al.*, 1995), and secrete *Tc*Cyp19 (Fig. S5A). In fact several cytosolic proteins including eIF5A and Hsp70 are found in the trypomastigote supernatant (data not shown) (Mandacaru *et al.*, 2019). In contrast cytoskeleton proteins such as β-tubulin was not released, indicating that the extracellular release was not caused by extensive cell death. Secretion of *Tc*Cyp19 and other cytosolic components was also observed when the trypomastigotes were incubated in the medium lacking glucose and/or FBS (data not shown), suggesting that *T. cruzi* is sensitive to changes in its environment and that cellular stresses could trigger the secretion of *Tc*Cyp19 and other cytosolic proteins. However, we could not detect parasite eIF5A in the cytosolic fraction of infected cells, arguing that different releasing mechanisms might occur in the intracellular amastigotes. For example, trypomastigotes release extracellular vesicles containing *Tc*Cyp19 (Ribeiro *et al.*, 2018) and whether vesicles are released by intracellular amastigotes is still unknown.

*Tc*Cyp19 secretion in amastigotes could only be detected by immunofluorescence 48 hr after parasite invasion, which suggests that the observed effects occur when high levels accumulate in the host cytoplasm. We cannot exclude, however, that *Tc*Cyp19 release started earlier. Interestingly, several reports have related that other functionally important *T. cruzi* proteins are secreted into the host cell cytosol by intracellular amastigotes; the intracellular phosphoinositide phospholipase C protein, a protein linked to the membrane by acyl chains, is released at the end of the intracellular development of *T. cruzi* (de Paulo Martins *et al.*, 2010). In addition, amastigote surface proteins such as Ssp-4 (Barros *et al.*, 1996), as well as the release of trans-sialidase by parasites undergoing differentiation as shown by (Frevert *et al.*, 1992).

Our results additionally provide evidence that overexpression of *Tc*Cyp19 by parasites and in L6 cells promotes increases amastigote proliferation. No differences were observed for invasion and early infection, suggesting that the observed effects occur essentially within the cytosol of the host cells. Increased secretion of *Tc*Cyp19 at 48 hr after infection coincide with the augmented growth. We cannot eliminate the possibility that *Tc*Cyp19 overexpression also influences biological events inside amastigotes that promoted its

proliferation. However, as the epimastigote proliferation did not change, and the expression of *Tc*Cyp19 in host cells cytosol enhances amastigote proliferation, this indicates a response primarily from *Tc*Cyp19 released by the parasite.

Expression of *Tc*Cyp19 in mammalian cells induces ROS increase, as shown for the mammalian CypA (Satoh *et al.*, 2010). Furthermore, the observed ROS increase by *Tc*Cyp19 was abolished by CsA, which inhibits cyclophilins. Consequently, the augmented ROS level induced by *Tc*Cyp19 explains how agents that increase ROS promote intracellular parasite proliferation (Finzi *et al.*, 2004; Goes *et al.*, 2016; Vilar-Pereira *et al.*, 2016; Dias *et al.*, 2017). In addition, depletion of *Tc*Cyp19 in the parasites decrease parasite growth and ROS production, and both could be reestablished with re-expression of *Tc*Cyp19 in add-back parasites. The role of *Tc*Cyp19 was additionally confirmed by using CAT-PEG, SOD-PEG, or CSA, known to reduce parasite multiplication (Bua *et al.*, 2004; Goes *et al.*, 2016; Dias *et al.*, 2017). These agents only diminished the number of intracellular amastigotes in L6 cells, infected with either control parasites, or the KD containing add-back constructs in comparison to *Tc*Cyp19 depleted line. This was even more evident in L6 expressing *Tc*Cyp19 after 96 hr post-infection, which strongly supports the hypothesis that the secreted *Tc*Cyp19 could be acting as CypA, inducing increased ROS levels. The reason why the growth effect is detected after 72 hr in the L6 infection model is not clearly understood. A different situation could occur in macrophages, in which an increase in ROS is observed earlier (Goes *et al.*, 2016). One possibility is that the amount of released *Tc*Cyp19 only occurs later, or a critical threshold should be attained.

We also found that like CypA, *Tc*Cyp19 accumulates in leading edges of host cells and is distributed along with actin microfilaments, as shown for vascular smooth muscle cells treated with angiotensin II (Soe *et al.*, 2013). Our confocal and super-resolution images suggest that *Tc*Cyp19 may chaperone this subunit to activate NOX2. This idea is compatible with findings showing that CypA helps translocation through the cell microfilaments to caveolae to generate the active NOX2 enzymatic complex, formed by the assembling of the proteins $p22^{phox}$, $p40^{phox}$, $p67^{phox}$ and Rac1, together with the transmembrane catalytic subunit $GP91^{phox}$ (Bedard *et al.*, 2007). The peculiar stria of *Tc*Cyp19-HA labeling, visible by super-resolution STED confocal microscopy analysis, supports the hypothesis that *Tc*Cyp19 may chaperone the $p47^{phox,}$ visible as punctate arrays enriched close to membrane-edges. Moreover, we found a correlation between the state of phosphorylation of $p47^{phox}$ and the presence of *Tc*Cyp19. In fact, one of the major functions of CypA is to promote retrograde transport of soluble proteins by association with the cytoskeleton (Galigniana *et al.*, 2004). The mechanism by which CypA, and also *Tc*Cyp19 acts on $p47^{phox}$ protein structure is unknown, however, they may bind to and isomerize proline residues in the proline reach region (PRR) of $p47^{phox}$ (El-Benna *et al.*, 2009), which is a known function of cyclophilins (Wang *et al.*, 2005). It is striking our finding that in the presence of cyclosporin, an inhibitor of cyclophilin caused accumulation of phosphorylated $p47^{phox}$ surrounding the cell nucleus which also colocalizes with *Tc*Cyp19, further supporting the notion that the proline isomerization is required to adequate transfer of $p47^{phox}$ to the cell edge.

Cyclophilins are highly conserved (Singh *et al.*, 2018), and it is not surprising that the cytosolic *Tc*Cyp19, which is the most abundant parasite cyclophilin, is similar to human CypA, despite the long evolutionary distance between these species. It is notable that the post-translational modification sites and regulatory residues are shared between *T. cruzi* and mammals CypA. Therefore, it is expected that the secretion of *Tc*Cyp19 by the parasite will produce similar effects observed by CypA in mammalian cells (Nigro *et al.*, 2013; Satoh, 2015; Xue *et al.*, 2018). Furthermore, it is possible that newly developed cyclophilin inhibitors to treat viral infections (Hopkins *et al.*, 2012) could also be effective in Chagas disease. Cyclophilins are protein chaperones with PPIase activity. Therefore, in the host cytoplasm, they could also bind to and modify other host cytosolic proteins to generate ROS.

In summary, our findings demonstrate that *Tc*Cyp19 is released in the cytosol of infected mammalian cells and induces ROS production, resulting in *T. cruzi* proliferation. This process appears relevant after a few parasite divisions and provides an environment to support further parasite proliferation (Fig. 10). These findings open new possibilities for dealing with Chagas disease, highlighting a factor involved in the parasite establishment in the mammalian host. It also supports the use of non-immunosuppressing inhibitors of cyclophilins as chemotherapy agents for the disease.

Supplementary Material

Refer to Web version on PubMed Central for supplementary material.

ACKNOWLEDGMENTS

We would like to thank Mariana Leão de Lima Stein, Claudio Rogerio Oliveira and Claudeci Medeiros da Costa for their excellent technical help. We are grateful to Prof. Francisco Rafael Martins Laurindo from the University of São Paulo for providing antibodies ($P47^{Phox}$) and for discussions and suggestions, Dr. Piero Banaresi and the Leica Microsystems team in Brazil for the help in the use of the STED microscope from the Instituto de Biociências da Universidade de São Paulo, Prof. Renato A. Mortara for immunofluorescence protocols and the use of the Confocal at the Universidade Federal de São Paulo, Dr. Thaysa Paschoalin, Dr. Tarciso Almeida Sellani at the Universidade Federal de São Paulo for help with cell migration assays, Dr. Lia Carolina S. Medeiros for providing the plasmids to express the recombinant SaCas9 and the plasmids to express the sgRNA, Dr. Roberto Docampo and Noelia Lander (University of Georgia, Athens) for providing the pTREX plasmids, and Dr. James Hunter, Universidade Federal de São Paulo, for some of the statistical analysis.

Funding Information

Fundação de Amparo à Pesquisa do Estado de São Paulo (2015/20031–0, 2018/09948–0, 2018/07766–2, 2017/02416–0 and 2017/19303–4); CNPq (445655/2014–3, 424729/2018–0 and by the INCTV-CNPq); American Heart Association (Grant-in-Aid-14GRNT20380635); National Institutes of Health (NIH, NIAID, R21AI131227–02); Drug for Neglected Diseases Initiative.

REFERENCES

Abuin G, Freitas L, Colli W, Alves M and Schenkman S (1999). Expression of trans-sialidase and 85-kDa glycoprotein genes in *Trypanosoma cruzi* is differentially regulated at the post-transcriptional level by labile protein factors. J Biol Chem 274: 13041–13047. [PubMed: 10224055]

Bangs JD, Uyetake L, Brickman MJ, Balber AE and Boothroyd JC (1993). Molecular cloning and cellular localization of a BiP homologue in *Trypanosoma brucei*. Divergent ER retention signals in a lower eukaryote. J Cell Sci 105: 1101–1113. [PubMed: 8227199]

Barbosa Leite A, Severo Gomes AA, de Castro Nascimento de Souza AC, Roberto de Mattos Fontes M, Schenkman S and Silvio Moretti N (2020). Effect of lysine acetylation on the regulation of *Trypanosoma brucei* glycosomal aldolase activity. Biochem J.

Barros HC, Da Silva S, Verbisck NV, Araguth MF, Tedesco RC, Procopio DO and Mortara RA (1996). Release of membrane-bound trails by *Trypanosoma cruzi* amastigotes onto modified surfaces and mammalian cells. J Euk Microbiol 43: 275–285. [PubMed: 8768431]

Bedard K and Krause KH (2007). The NOX family of ROS-generating NADPH oxidases: physiology and pathophysiology. Physiol Rev 87: 245–313. [PubMed: 17237347]

Bonney KM and Engman DM (2008). Chagas heart disease pathogenesis: one mechanism or many? Curr Mol Med 8: 510–518. [PubMed: 18781958]

Bua J, Aslund L, Pereyra N, Garcia GA, Bontempi EJ and Ruiz AM (2001). Characterisation of a cyclophilin isoform in *Trypanosoma cruzi*. FEMS Microbiol Lett 200: 43–47. [PubMed: 11410347]

Bua J, Fichera LE, Fuchs AG, Potenza M, Dubin M, Wenger RO, et al. (2008). Anti-*Trypanosoma* cruzi effects of cyclosporin A derivatives: possible role of a P-glycoprotein and parasite cyclophilins. Parasitology 135: 217–228. [PubMed: 17922928]

Bua J, Ruiz AM, Potenza M and Fichera LE (2004). In vitro anti-parasitic activity of Cyclosporin A analogs on *Trypanosoma cruzi*. Biorg Med Chem Lett 14: 4633–4637.

Bustos PL, Perrone AE, Milduberger N, Postan M and Bua J (2015). Oxidative stress damage in the protozoan parasite *Trypanosoma cruzi* is inhibited by Cyclosporin A. Parasitology 142: 1024–1032. [PubMed: 25823521]

Camargo EP (1964). Growth and Differentiation in *Trypanosoma cruzi*. I. Origin of Metacyclic Trypanosomes in Liquid Media. Rev Inst Med Trop Sao Paulo 6: 93–100. [PubMed: 14177814]

Carraro R, Bua J, Ruiz A and Paulino M (2007). Modelling and study of cyclosporin A and related compounds in complexes with a *Trypanosoma cruzi* cyclophilin. J Mol Graph Model 26: 48–61. [PubMed: 17174582]

Carraro R, Iribarne F and Paulino M (2016). Analysis of cyclosporin A and a set of analogs as inhibitors of a *T. cruzi* cyclophilin by docking and molecular dynamics. J Biomol Struct Dyn 34: 399–413. [PubMed: 26046477]

Chung J, Rocha AA, Tonelli RR, Castilho BA and Schenkman S (2013). Eukaryotic initiation factor 5A dephosphorylation is required for translational arrest in stationary phase cells. Biochem J 451: 257–267. [PubMed: 23368777]

Contreras VT, Salles JM, Thomas N, Morel CM and Goldenberg S (1985). In vitro differentiation of *Trypanosoma cruzi* under chemically defined conditions. Mol Biochem Parasitol 16: 315–327. [PubMed: 3903496]

Cunha-Neto E, Teixeira PC, Nogueira LG and Kalil J (2011). Autoimmunity. Adv Parasitol 76: 129–152. [PubMed: 21884890]

Davis TL, Walker JR, Campagna-Slater V, Finerty PJ, Paramanathan R, Bernstein G, et al. (2010). Structural and biochemical characterization of the human cyclophilin family of peptidyl-prolyl isomerases. Plos Biol 8: e1000439. [PubMed: 20676357]

de Paulo Martins V, Okura M, Maric D, Engman DM, Vieira M, Docampo R and Moreno SN (2010). Acylation-dependent export of *Trypanosoma cruzi* phosphoinositide-specific phospholipase C to the outer surface of amastigotes. J Biol Chem 285: 30906–30917. [PubMed: 20647312]

Dhiman M and Garg NJ (2011). NADPH oxidase inhibition ameliorates *Trypanosoma cruzi*-induced myocarditis during Chagas disease. J Pathol 225: 583–596. [PubMed: 21952987]

Dias PP, Capila RF, do Couto NF, Estrada D, Gadelha FR, Radi R, et al. (2017). Cardiomyocyte oxidants production may signal to *T. cruzi* intracellular development. Plos Negl Trop Dis 11: e0005852. [PubMed: 28832582]

Dornan J, Taylor P and Walkinshaw MD (2003). Structures of immunophilins and their ligand complexes. Curr Top Med Chem 3: 1392–1409. [PubMed: 12871171]

El-Benna J, Dang PM, Gougerot-Pocidalo MA, Marie JC and Braut-Boucher F (2009). p47phox, the phagocyte NADPH oxidase/NOX2 organizer: structure, phosphorylation and implication in diseases. Exp Mol Med 41: 217–225. [PubMed: 19372727]

Estrada D, Specker G, Martinez A, Dias PP, Hissa B, Andrade LO, et al. (2018). Cardiomyocyte diffusible redox mediators control *Trypanosoma cruzi* infection: role of parasite mitochondrial iron superoxide dismutase. Biochem J 475: 1235–1251. [PubMed: 29438066]

Finzi JK, Chiavegatto CW, Corat KF, Lopez JA, Cabrera OG, Mielniczki-Pereira AA, et al. (2004). *Trypanosoma cruzi* response to the oxidative stress generated by hydrogen peroxide. Mol Biochem Parasitol 133: 37–43. [PubMed: 14668010]

Fischer G and Aumuller T (2003). Regulation of peptide bond cis/trans isomerization by enzyme catalysis and its implication in physiological processes. Rev Physiol Biochem Pharmacol 148: 105–150. [PubMed: 12698322]

Frevert U, Schenkman S and Nussenzweig V (1992). Stage-specific expression and intracellular shedding of the cell surface trans-sialidase of *Trypanosoma cruzi*. Infect Immun 60: 2349–2360. [PubMed: 1375197]

Galigniana MD, Morishima Y, Gallay PA and Pratt WB (2004). Cyclophilin-A is bound through its peptidylprolyl isomerase domain to the cytoplasmic dynein motor protein complex. J Biol Chem 279: 55754–55759. [PubMed: 15496417]

Goes GR, Rocha PS, Diniz AR, Aguiar PH, Machado CR and Vieira LQ (2016). *Trypanosoma cruzi* Needs a Signal Provided by Reactive Oxygen Species to Infect Macrophages. Plos Negl Trop Dis 10: e0004555. [PubMed: 27035573]

Heinzmann D, Bangert A, Muller AM, von Ungern-Sternberg SN, Emschermann F, Schonberger T, et al. (2015). The Novel Extracellular Cyclophilin A (CyPA) - Inhibitor MM284 Reduces Myocardial Inflammation and Remodeling in a Mouse Model of Troponin I -Induced Myocarditis. PLoS One 10: e0124606. [PubMed: 25894208]

Hopkins S and Gallay P (2012). Cyclophilin inhibitors: an emerging class of therapeutics for the treatment of chronic hepatitis C infection. Viruses 4: 2558–2577. [PubMed: 23202494]

Kulkarni MM, Karafova A, Kamysz W, Schenkman S, Pelle R and McGwire BS (2013). Secreted trypanosome cyclophilin inactivates lytic insect defense peptides and induces parasite calcineurin activation and infectivity. J Biol Chem 288: 8772–8784. [PubMed: 23386612]

Lander N, Li ZH, Niyogi S and Docampo R (2015). CRISPR/Cas9-Induced Disruption of Paraflagellar Rod Protein 1 and 2 Genes in *Trypanosoma cruzi* Reveals Their Role in Flagellar Attachment. MBio 6.

Malesevic M, Gutknecht D, Prell E, Klein C, Schumann M, Nowak RA, et al. (2013). Anti-inflammatory effects of extracellular cyclosporins are exclusively mediated by CD147. J Med Chem 56: 7302–7311. [PubMed: 23964991]

Mandacaru SC, Queiroz RML, Alborghetti MR, de Oliveira LS, de Lima CMR, Bastos IMD, et al. (2019). Exoproteome profiling of *Trypanosoma cruzi* during amastigogenesis early stages. PLoS One 14: e0225386. [PubMed: 31756194]

McDowell MA, Ransom DM and Bangs JD (1998). Glycosylphosphatidylinositol-dependent secretory transport in *Trypanosoma brucei*. Biochem J 335: 681–689. [PubMed: 9794811]

Meijles DN, Fan LM, Howlin BJ and Li JM (2014). Molecular insights of p47phox phosphorylation dynamics in the regulation of NADPH oxidase activation and superoxide production. J Biol Chem 289: 22759–22770. [PubMed: 24970888]

Moretti NS, Cestari I, Anupama A, Stuart K and Schenkman S (2017). Comparative Proteomic Analysis of Lysine Acetylation in Trypanosomes. J Prote Res 17: 374–385.

Nigro P, Pompilio G and Capogrossi MC (2013). Cyclophilin A: a key player for human disease. Cell Death Dis 4: e888. [PubMed: 24176846]

Nigro P, Satoh K, O'Dell MR, Soe NN, Cui Z, Mohan A, et al. (2011). Cyclophilin A is an inflammatory mediator that promotes atherosclerosis in apolipoprotein E-deficient mice. J Exp Med 208: 53–66. [PubMed: 21173104]

Paiva CN and Bozza MT (2014). Are reactive oxygen species always detrimental to pathogens? Antioxid Redox Signal 20: 1000–1037. [PubMed: 23992156]

Paiva CN, Feijo DF, Dutra FF, Carneiro VC, Freitas GB, Alves LS, et al. (2012). Oxidative stress fuels *Trypanosoma cruzi* infection in mice. J Clin Invest 122: 2531–2542. [PubMed: 22728935]

Paiva CN, Medei E and Bozza MT (2018). ROS and *Trypanosoma cruzi*: Fuel to infection, poison to the heart. PLoS Pathog 14: e1006928. [PubMed: 29672619]

Pelle R, McOdimba F, Chuma F, Wasawo D, Pearson TW and Murphy NB (2002). The African trypanosome cyclophilin A homologue contains unusual conserved central and N-terminal domains and is developmentally regulated. Gene 290: 181–191. [PubMed: 12062813]

Peng D and Tarleton R (2015). EuPaGDT: a web tool tailored to design CRISPR guide RNAs for eukaryotic pathogens. Microb Genom 1: e000033. [PubMed: 28348817]

Potenza M, Galat A, Minning TA, Ruiz AM, Duran R, Tarleton RL, et al. (2006). Analysis of the *Trypanosoma cruzi* cyclophilin gene family and identification of Cyclosporin A binding proteins. Parasitology 132: 867–882. [PubMed: 16700961]

Ramirez MI, Yamauchi LM, de Freitas LH Jr., Uemura H and Schenkman S (2000). The use of the green fluorescent protein to monitor and improve transfection in *Trypanosoma cruzi*. Mol Biochem Parasitol 111: 235–240. [PubMed: 11087935]

Ran FA, Cong L, Yan WX, Scott DA, Gootenberg JS, Kriz AJ, et al. (2015). In vivo genome editing using *Staphylococcus aureus* Cas9. Nature 520: 186–191. [PubMed: 25830891]

Rego JV, Duarte AP, Liarte DB, de Carvalho Sousa F, Barreto HM, Bua J, et al. (2015). Molecular characterization of Cyclophilin (TcCyP19) in *Trypanosoma cruzi* populations susceptible and resistant to benznidazole. Exp Parasitol 148: 73–80. [PubMed: 25450774]

Ren YX, Wang SJ, Fan JH, Sun SJ, Li X, Padhiar AA and Zhang JN (2016). CD147 stimulates hepatoma cells escaping from immune surveillance of T cells by interaction with Cyclophilin A. Biomed Pharmacother 80: 289–297. [PubMed: 27133068]

Ribeiro KS, Vasconcellos CI, Soares RP, Mendes MT, Ellis CC, Aguilera-Flores M, et al. (2018). Proteomic analysis reveals different composition of extracellular vesicles released by two *Trypanosoma cruzi* strains associated with their distinct interaction with host cells. J Extracell Ves 7: 1463779.

Satoh K (2015). Cyclophilin A in cardiovascular homeostasis and diseases. Tohoku J Exp Med 235: 1–15. [PubMed: 25743766]

Satoh K, Nigro P, Matoba T, O'Dell MR, Cui Z, Shi X, et al. (2009). Cyclophilin A enhances vascular oxidative stress and the development of angiotensin II-induced aortic aneurysms. Nat Med 15: 649–656. [PubMed: 19430489]

Satoh K, Shimokawa H and Berk BC (2010). Cyclophilin A: promising new target in cardiovascular therapy. Circ J 74: 2249–2256. [PubMed: 20962430]

Schiene-Fischer C (2014). Multidomain peptidyl prolyl cis/trans Isomerases. Biochim Biophys Acta.

Seizer P, Ungern-Sternberg SN, Schonberger T, Borst O, Munzer P, Schmidt EM, et al. (2015). Extracellular cyclophilin A activates platelets via EMMPRIN (CD147) and PI3K/Akt signaling, which promotes platelet adhesion and thrombus formation in vitro and in vivo. Arterioscler Thromb Vasc Biol 35: 655–663. [PubMed: 25550208]

Singh K, Winter M, Zouhar M and Rysanek P (2018). Cyclophilins: Less Studied Proteins with Critical Roles in Pathogenesis. Phytopathology 108: 6–14. [PubMed: 28643580]

Soares Medeiros LC, South L, Peng D, Bustamante JM, Wang W, Bunkofske M, et al. (2017). Rapid, Selection-Free, High-Efficiency Genome Editing in Protozoan Parasites Using CRISPR-Cas9 Ribonucleoproteins. MBio 8.

Soe NN, Sowden M, Baskaran P, Kim Y, Nigro P, Smolock EM and Berk BC (2014). Acetylation of cyclophilin A is required for its secretion and vascular cell activation. Cardiovasc Res 101: 444–453. [PubMed: 24293519]

Soe NN, Sowden M, Baskaran P, Smolock EM, Kim Y, Nigro P and Berk BC (2013). Cyclophilin A is required for angiotensin II-induced p47phox translocation to caveolae in vascular smooth muscle cells. Arterioscler Thromb Vasc Biol 33: 2147–2153. [PubMed: 23846495]

Suzuki J, Jin ZG, Meoli DF, Matoba T and Berk BC (2006). Cyclophilin A is secreted by a vesicular pathway in vascular smooth muscle cells. Circ Res 98: 811–817. [PubMed: 16527992]

Tomlinson S, Vandekerckhove F, Frevert U and Nussenzweig V (1995). The induction of *Trypanosoma cruzi* trypomastigote to amastigote transformation by low pH. Parasitology 110: 547–554. [PubMed: 7541124]

Vilar-Pereira G, Carneiro VC, Mata-Santos H, Vicentino AR, Ramos IP, Giarola NL, et al. (2016). Resveratrol Reverses Functional Chagas Heart Disease in Mice. Plos Pathog 12: e1005947. [PubMed: 27788262]

Wang P and Heitman J (2005). The cyclophilins. Genome Biology 6: 226. [PubMed: 15998457]

Wen JJ, Gupta S, Guan Z, Dhiman M, Condon D, Lui C and Garg NJ (2010). Phenyl-alpha-tert-butyl-nitrone and benzonidazole treatment controlled the mitochondrial oxidative stress and evolution of cardiomyopathy in chronic chagasic Rats. Journal of the American College of Cardiology 55: 2499–2508. [PubMed: 20510218]

Wen JJ, Nagajyothi F, Machado FS, Weiss LM, Scherer PE, Tanowitz HB and Garg NJ (2014). Markers of oxidative stress in adipose tissue during *Trypanosoma cruzi* infection. Parasitol Res 113: 3159–3165. [PubMed: 24948102]

Xue C, Sowden MP and Berk BC (2018). Extracellular and Intracellular Cyclophilin A, Native and Post-Translationally Modified, Show Diverse and Specific Pathological Roles in Diseases. Arterioscler Thromb Vasc Biol 38: 986–993. [PubMed: 29599134]

Take away

1. *T. cruzi* express a major cyclophilin (*Tc*Cyp19) in all parasite stages.
2. *Tc*Cyp19 is secreted by intracellular amastigotes in the host cytosol.
3. The presence of *Tc*Cyp19 secreted or expressed exogenously is sufficient to increase intracellular proliferation.
4. The presence of *Tc*Cyp19 causes an increase in cellular ROS which causes the increased proliferation.
5. *Tc*Cyp19 may cause ROS increase by interacting with the $p47^{phox}$ to activate the NADPH oxidase (Nox2).

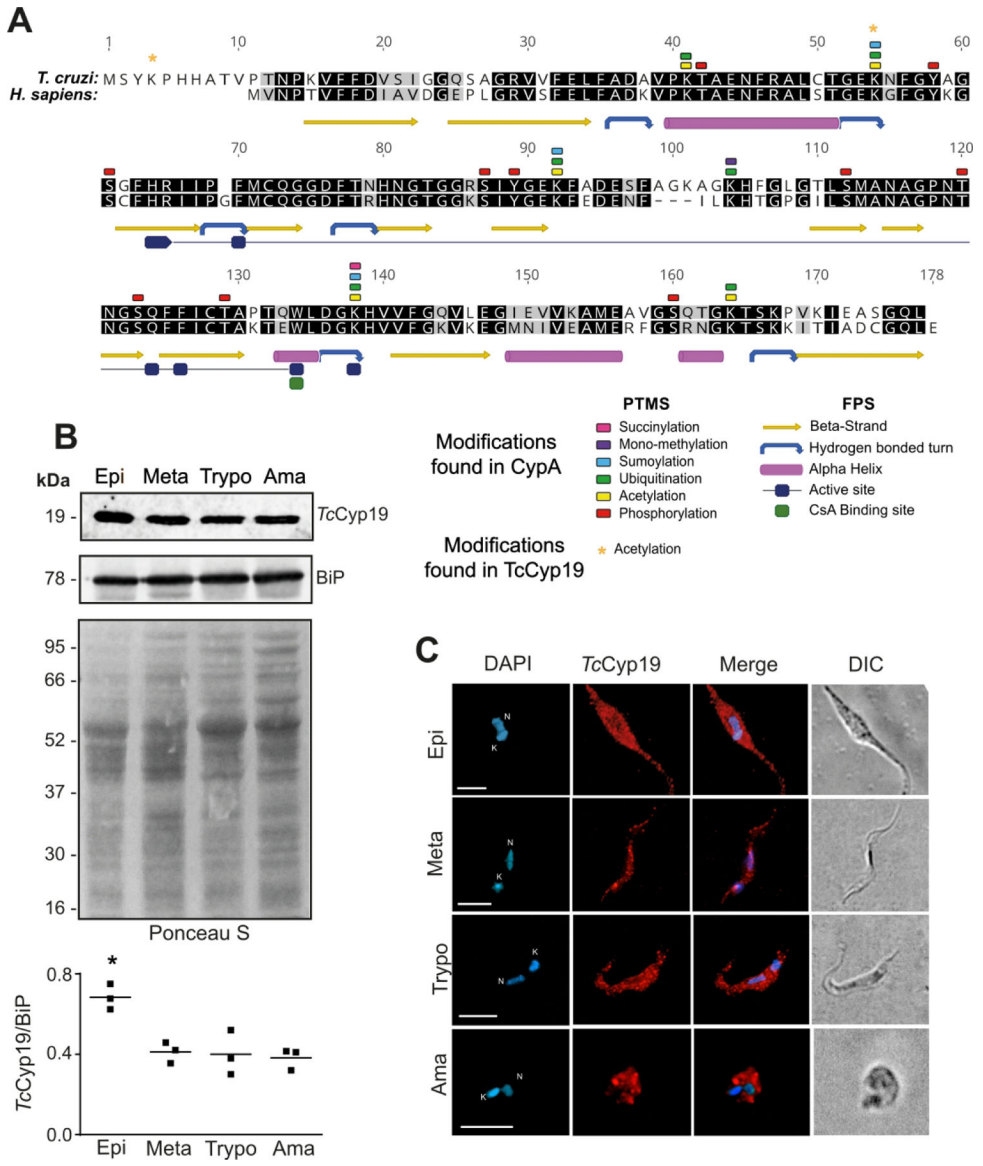

Figure 1. *Tc*CyP19 is similar to mammalian CypA, conserves the main post-translation modification sites and is expressed in the cytosol of all *T. cruzi* stages.

(A) Clustal-W alignment of amino acid sequence of *Tc*CypP9 (TcCLB.506925.300) and human CypA (PPIA HUMAN) indicating its post-translational modification sites (PTMS) and the folding features (FPS) (P62937 at https://www.uniprot.org/). The numbers correspond to *Tc*Cyp19 sequence. (B) Western blot of *T. cruzi* total extracts containing 10 μg of proteins obtained from epimastigotes (Epi), metacyclic trypomastigotes (Meta), tissue cultured trypomastigotes (Trypo) and amastigotes (Ama) probed with anti-*Tc*CyP19 and anti-BiP antibodies. The bottom panel shows the nitrocellulose membrane stained by Ponceau S. The graph shows the relative means of *Tc*CyP19 to BiP intensity and standard deviation of three independent experiments. * indicates significantly different values ($p < 0.01$) of epimastigotes related to all other stages calculated using One-Way ANOVA with Dunnet correction. (C) Immunofluorescence labeling of *Tc*CyP19 in the *T. cruzi* stages. The cells were adsorbed to glass slides, fixed, permeabilized, and incubated with anti-*Tc*CyP19

antibodies (red) and DAPI (blue). The images also show merged fluorescent signals and the differential interference contrast (DIC). Bars = 5 μm. Nucleus (N) and kinetoplast (K).

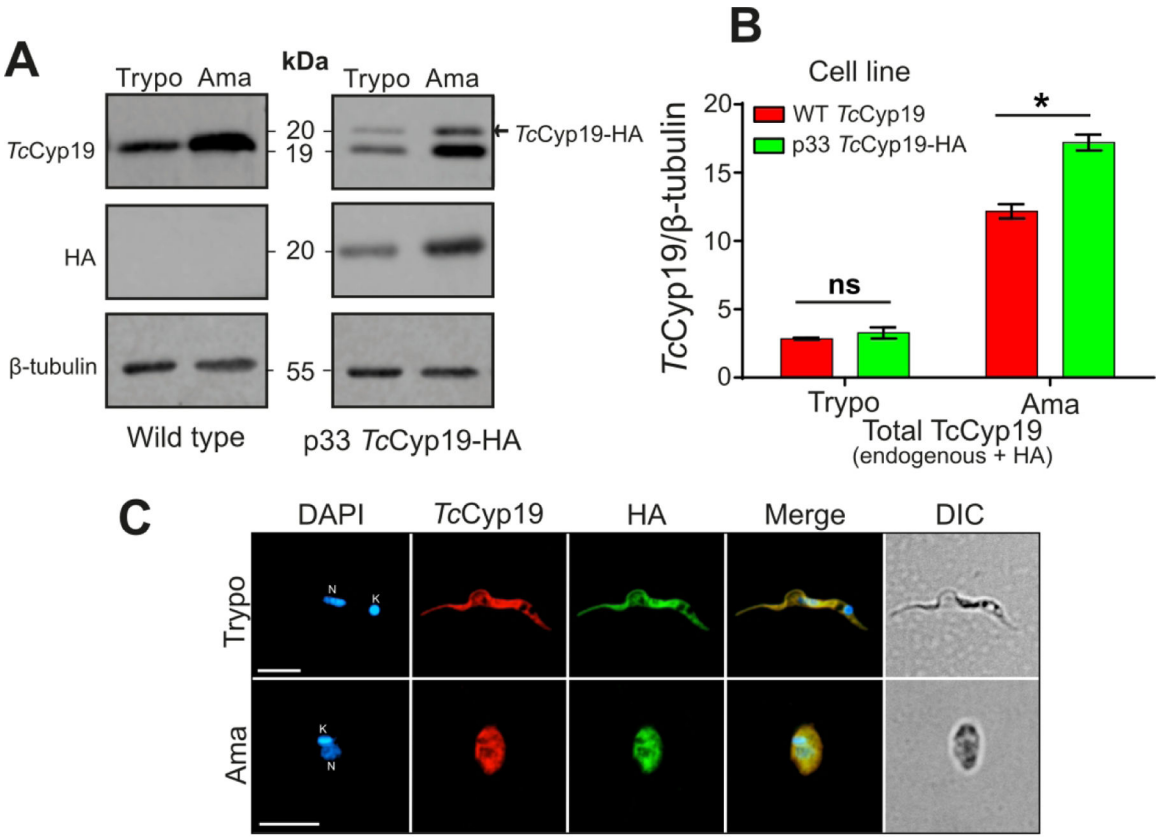

Figure 2. Generation of *T. cruzi* cell lineage expressing the HA-tagged *Tc*CyP19.

(A) Western blot of the total extracts containing 1×10^7 tissue culture trypomastigotes (Trypo) and 5×10^6 intracellular amastigotes (Ama) of non-transfected or parasites transfected with p33*Tc*CyP19-HA were separated by SDS-PAGE. The proteins were transferred to nitrocellulose membranes which were probed with anti-*Tc*CyP19, anti-HA, and anti-β-tubulin antibodies. (B) The graphic indicates the endogenous and exogenous *Tc*CyP19 / β-tubulin ratio in the wild type and p33*Tc*CyP19-HA parasites. The data represent the means ± standard deviation of three independent experiments. Asterisk indicates statistically significant differences ($p < 0.05$) based on Two-Way ANOVA, Sidak's test was applied. ns = non-significant. (C) Immunofluorescence showing tissue culture trypomastigotes (Trypo) and intracellular amastigotes (Ama) expressing *Tc*CyP19-HA. The parasites were adsorbed to glass slides, fixed, permeabilized, and incubated with anti-*Tc*CyP19 (red), anti-HA (green) antibodies, and DAPI (blue). The images show individual fluorescent labeling, fluorescence signals merged and differential interference contrast (DIC). Bars = 5 μm. Nucleus (N) and kinetoplast (K).

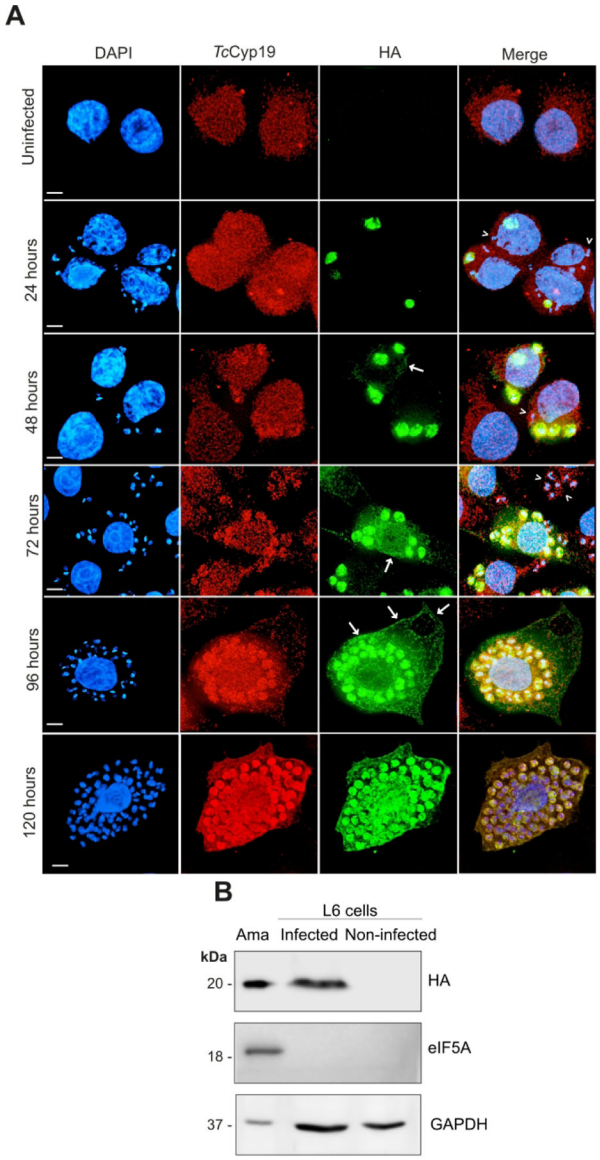

Figure 3. Intracellular amastigotes secrete *Tc*CyP19-HA into the host cell cytosol.

(A) Immunofluorescence of uninfected wild type L6 cells, or L6 cells infected with *T. cruzi* parasites expressing the *Tc*CyP19-HA. The images were obtained after glutaraldehyde-fixation protocol at the indicated hours after infection. The images show the DNA stained by DAPI (blue), anti-*Tc*CyP19 (red), anti-HA (green) antibodies, and the merged fluorescence. Arrows indicate the secretion labeling, and arrow-heads the wild type amastigotes not labeled with the anti-HA antibodies. Bars = 5 μm. (B). Infected and non-infected L6 cells in 150 cm^2 tissue culture flask were collected 120 hr after parasite addition and lysed in 1 mL PBS as described in Methods. One 60^{th} of the total volume was loaded in each lane and membranes were probed with anti-HA, anti-eIF5A and anti-human GAPDH. Purified intracellular amastigotes (5×10^6) was extracted from the infection (Ama) and was loaded as control.

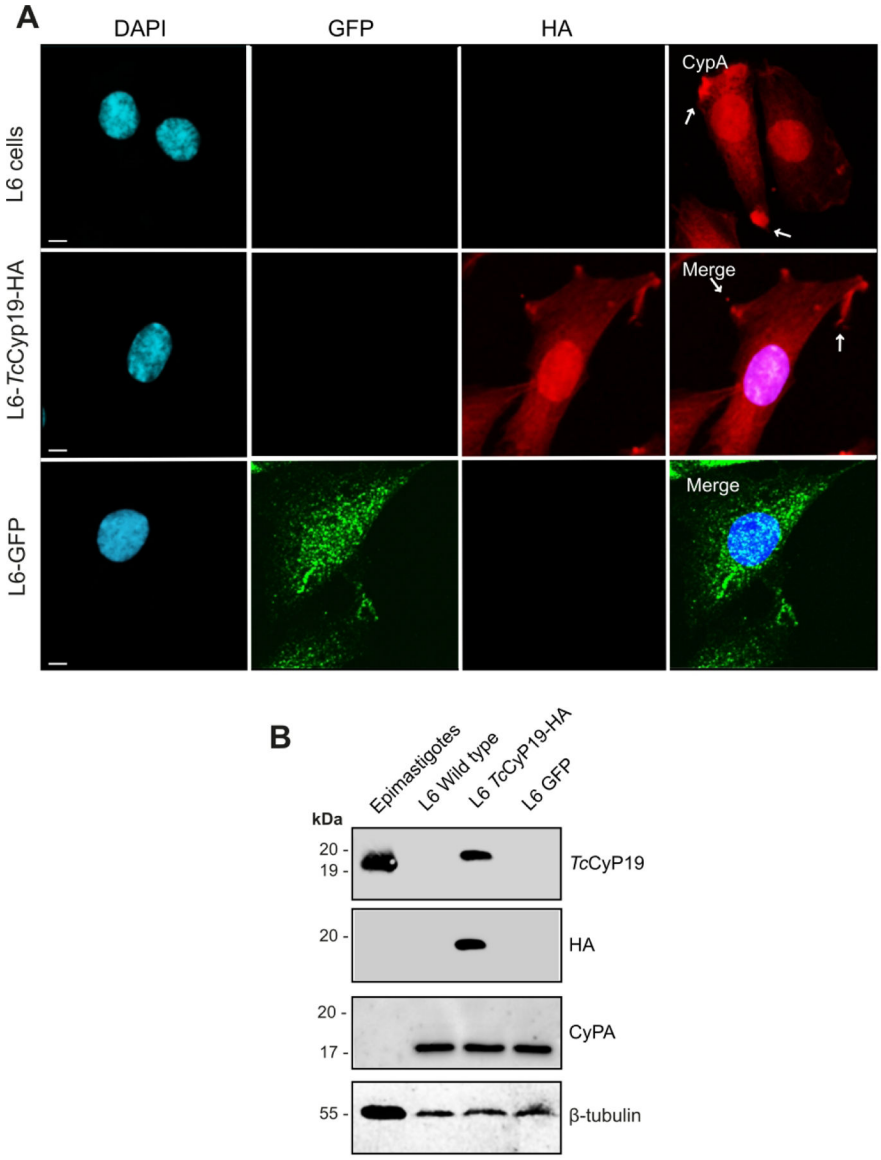

Figure 4. Expression of *Tc*CyP19-HA by myoblast L6 cells.

(A) L6 cells, L6 cells expressing *Tc*Cyp19-HA, or GFP, both in pCDNATO were plated on glass slides and after 24 hr, fixed, permeabilized, and incubated with anti-CypA (red), anti-HA (red), anti-GFP (green) and DAPI (blue). The images show individual labeling and the merged fluorescence signals. Arrows indicate the accumulation of both CypA and *Tc*Cyp19 in cell edges. Bars = 5 μm. (B) Western blot of a total extract of 2×10^6 epimastigotes (control) and wild type or transfected L6 cells, as indicated. Membranes were probed with anti-*Tc*Cyp19, anti-CypA, anti-HA and anti-β tubulin antibodies. Size markers are indicated in the left side of the gels.

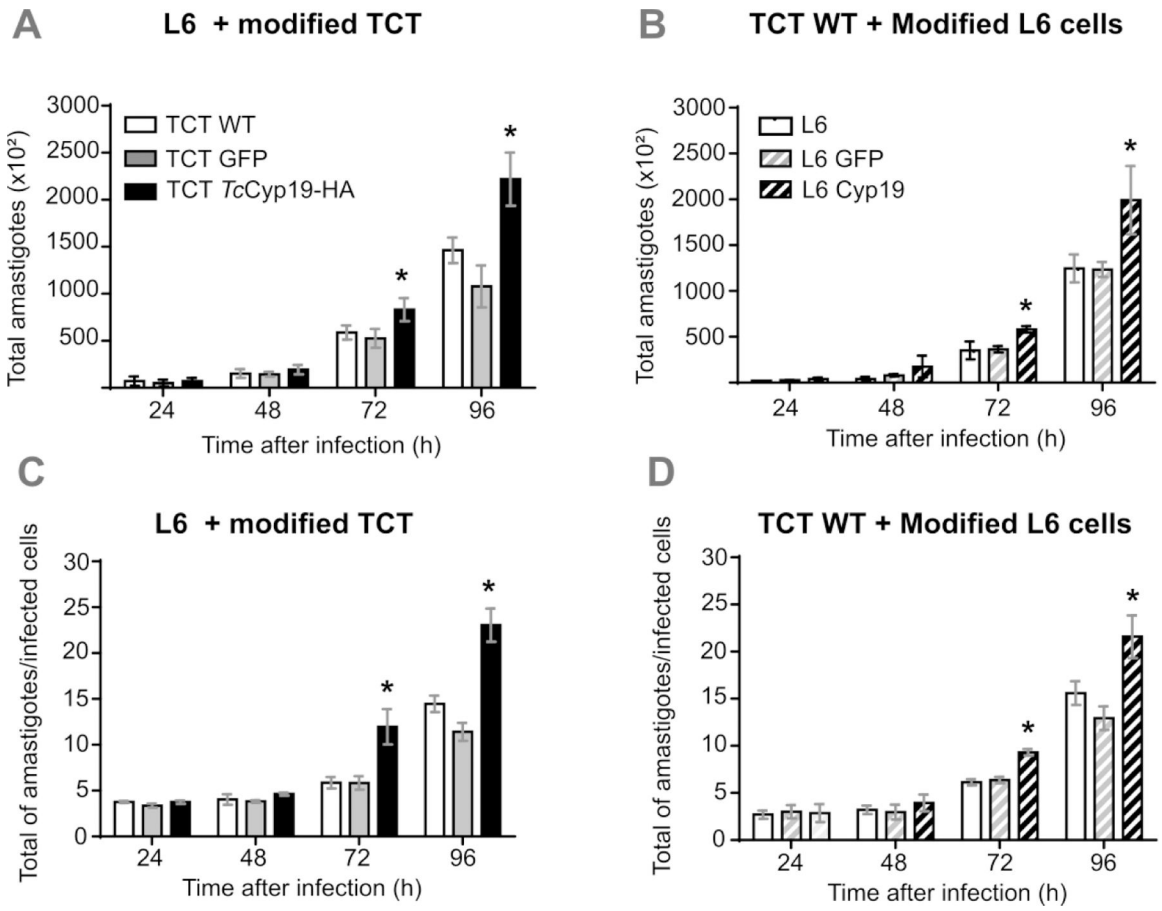

Figure 5. *Tc*Cyp19 expressed either in L6 cells or in parasites causes increased intracellular parasite growth.

Trypomastigotes of the designated lines (WT, GFP, or *Tc*Cyp19-HA) were added to L6 cells not expressing, expressing GFP or *Tc*Cyp19 in 96 well plates and the infection followed by imaging the cells after Draq5 stain, as detailed in Methods section. The graphs show the total number of amastigotes (A and B) and number of amastigotes per infected cell (C and D) from 24 to 96 hr post-infection. The data represent the means ± standard deviation of three independent experiments each done in triplicates. Asterisk indicates $p < 0.0001$,calculated using Two-Way ANOVA, with Sidak's post-test.

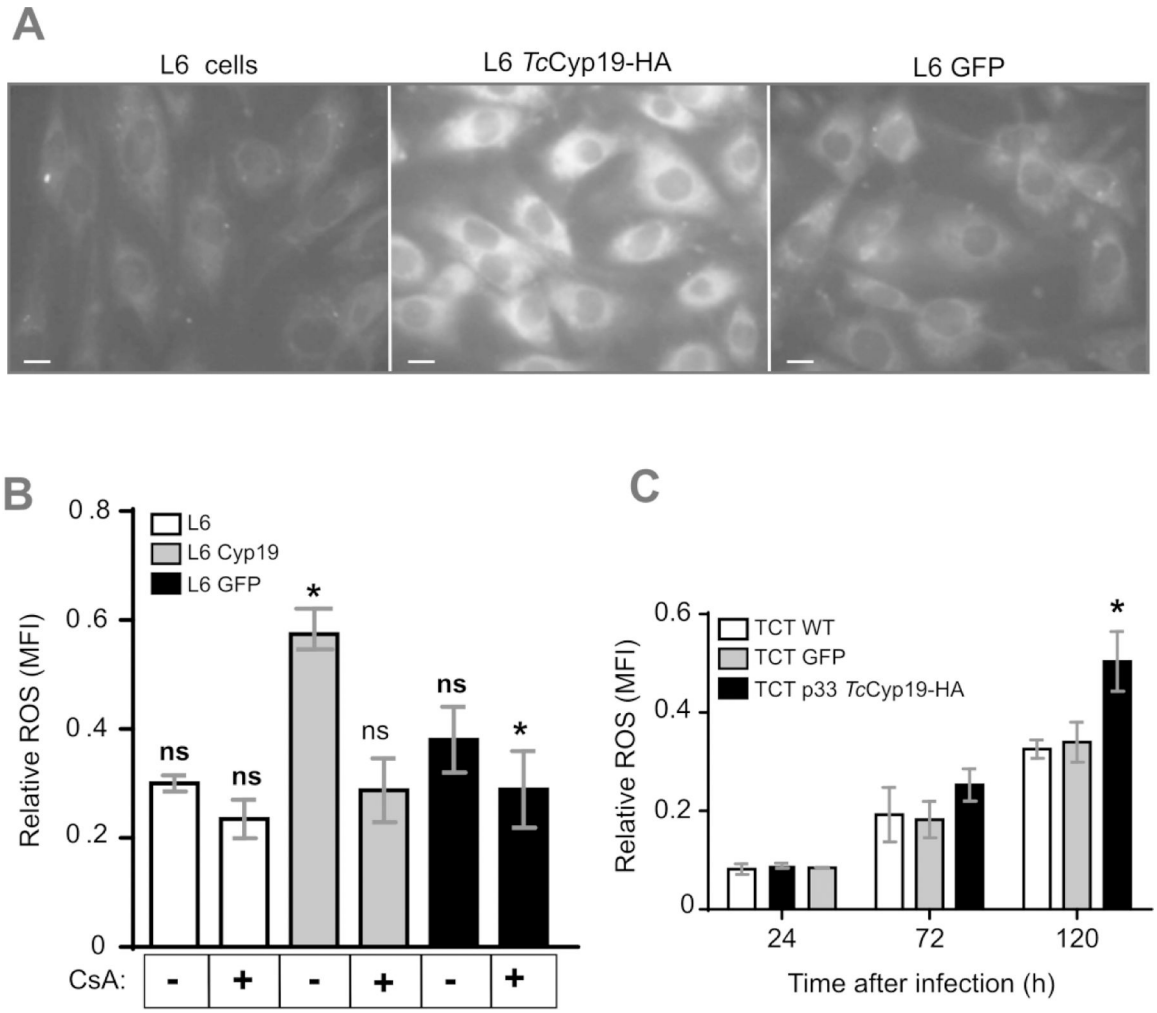

Figure 6. *Tc*Cyp19 increases ROS levels in L6 cells.

(A) Immunofluorescence detection of basal ROS production in L6 cells obtained from the oxidation of the CellROX-Deep Red probe. Bars = 5 μm. (B) ROS quantification in the indicated L6 cell lines by using the CM-H_2DCFDA probe before and after 15 hr pretreatment with 20 μM of ciclosporin A (CsA). (C) ROS production detected by CM-H_2DCFDA probe in wild type L6 cells at 24, 72 and 120 hr after the infection by the indicated tissue culture trypomastigotes. The bars represent relative levels ± standard deviation of ROS mean fluorescence intensity (MFI) of 3 independent experiments, each read in triplicate measurements. Asterisk indicates $p < 0.005$, by using One-Way and Two-Way Anova Sidak's and Turkey tests respectively for (B) and (C).

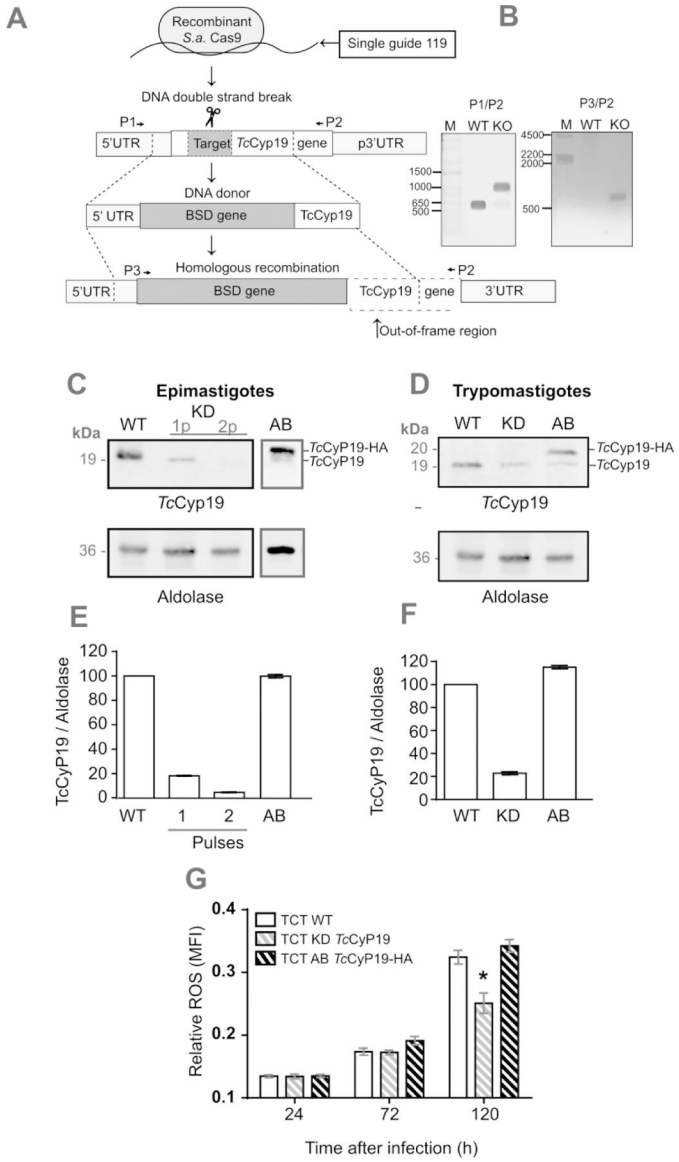

Figure 7. *Tc*Cyp19 depleted *T. cruzi* shows reduced ROS production upon cell infection.

(A) The panel shows the approach used to introduce the resistance to blasticidin (BSD) antibiotic gene in the *TcCyp19* ORF as described in the Methods section. (B) Confirmation of *Tc*Cyp19 deletion in epimastigotes by PCR using the primers P1/P2 to *Tc*Cyp19 gene amplification and P2/P3 to BSD gene insertion amplification. (C) Lysates of non-transfected (WT) epimastigote extracts obtained after one or two pulses (1p and 2p) within 5 days 30 days after transfection in the presence of 100 μg/mL of BSD to select the resistant lineages (KD). Lane AB shows a 2p epimastigote extract after insertion of p33*TcCyp19*-HA and further selection in 0.2 mg/mL geneticin G418. The parasites were analyzed by Western blotting probed with anti-*Tc*Cyp19 (top) or anti-aldolase antibodies (bottom panel). (D) Western blot of tissue culture trypomastigotes obtained from the wild type (WT), KD and AB probed with anti-*Tc*Cyp19 and anti-Aldolase antibodies. Graphs in E and F show the normalized means of *Tc*Cyp19/Aldolase ratios ± standard deviation (n = 3) respectively for

epimastigotes and trypomastigotes. (G) ROS production detected by CM-H_2DCFDA probe in control L6 cells at 24, 72 and 120 hr post infection by the indicated lines of trypomastigotes. The bars represent relative levels ± standard deviation of ROS mean fluorescence intensity (MFI) of 3 independent experiments, each read in triplicate measurements. Asterisk indicates $p < 0.005$, by using Two-Way Anova and Turkey tests.

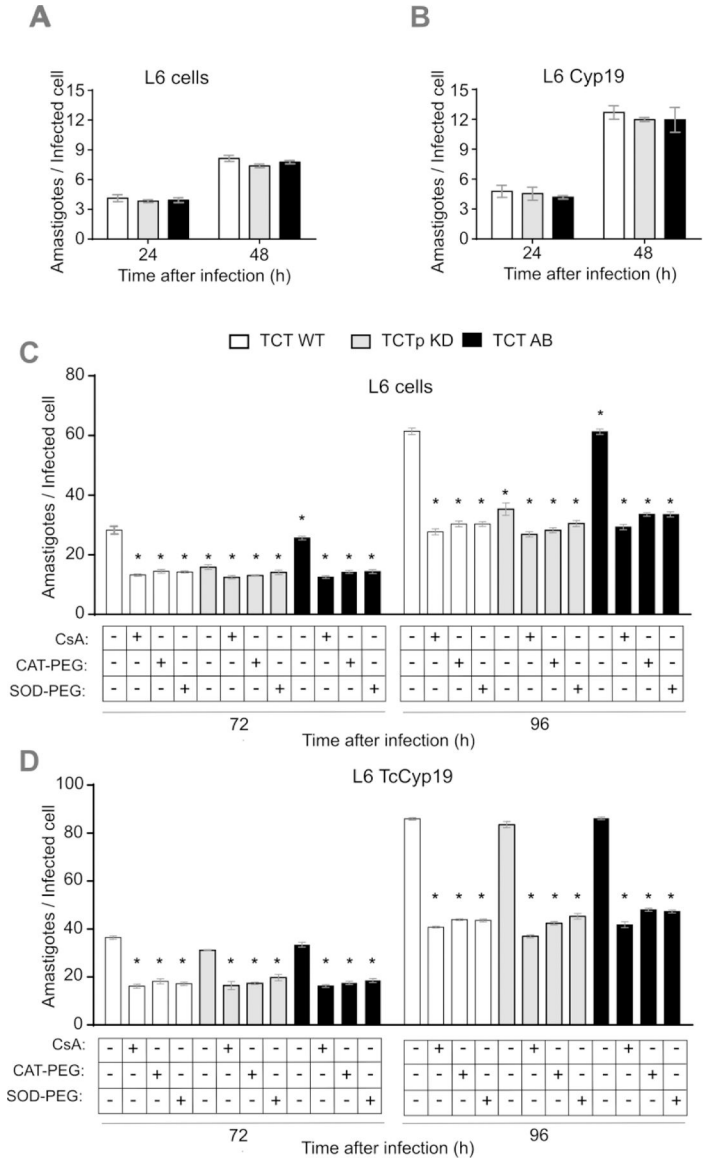

Figure 8. Depleted *Tc*Cyp19 parasites show reduced multiplication rate that is reverted in add-back parasites or in *Tc*Cyp19 expressing L6 cells.

WT, KD and AB tissue culture trypomastigotes were used to infect L6 cells plated on glass coverslips in 24 well plates at MOI = 20:1 in a volume of 500 μL for 6 h. The cells were then washed with PBS and incubations continued in 500 μL of fresh cDMEM medium. The wells were washed, and the coverslips were collected, fixed with 4% paraformaldehyde in PBS and stained with Hoechst 33342 at the indicated times after infection. The graphs show the total number of amastigotes per infected L6 cells (A) and L6 CyP19 cells (B) 24 to 48 hours post-infection. Control L6 (C) and L6 TCyP19 cells (D) were incubated as above and at 48 hr post-infection treated either with 20 μM cyclosporin A (CsA), 25 units of catalase-polyethylene glycol (CAT-PEG), or 20 units of superoxide dismutase-polyethylene glycol (SOD-PEG). The number of amastigotes per infected cells was determined 72 and 96 hr post-infection. The data represent the means ± standard deviation of three independent

experiments each done in triplicates. Asterisk indicates $p < 0.001$ when comparing the numbers relative to no additions and calculated by Two-Way ANOVA and Sidak's post-test.

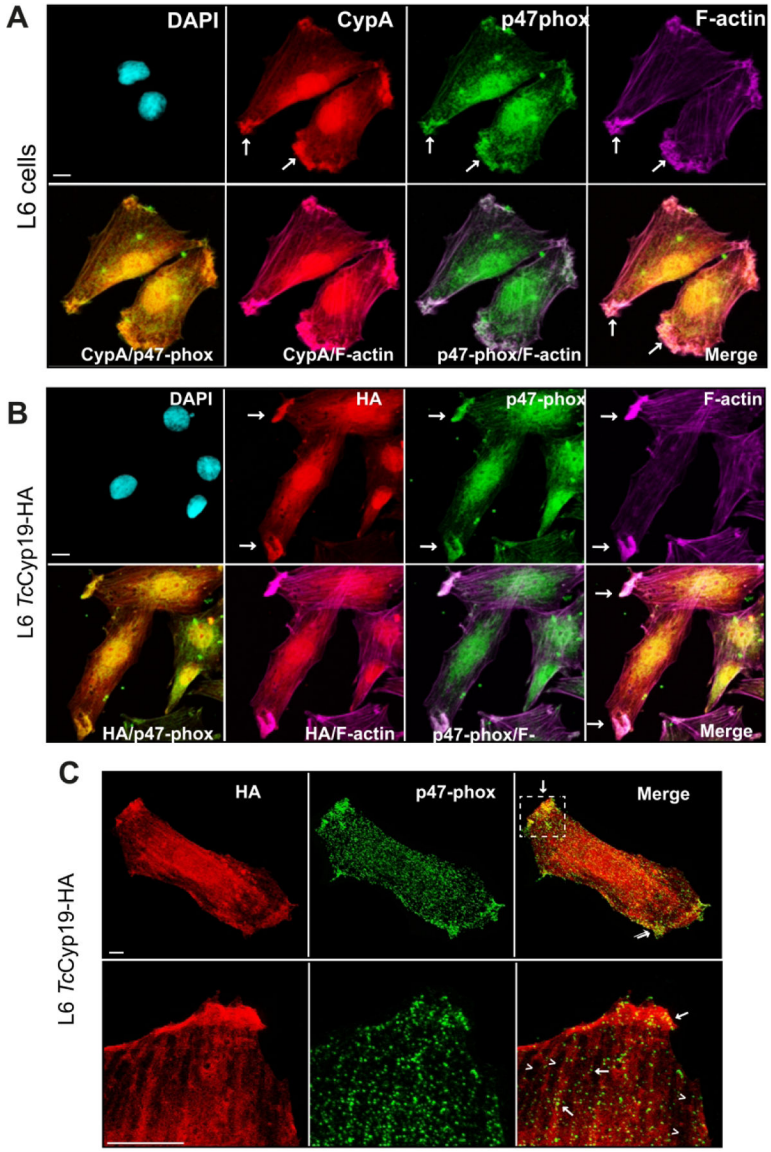

Figure 9. *Tc*Cyp19-HA and p47^{Phox} accumulate in leading edges of L6 myoblasts.

Representative immunofluorescence images obtained by staining L6 (A) and L6 expressing *Tc*Cyp19-HA with anti-CypA and anti-HA (red), anti-p47^{phox} (green), anti-F-actin (purple) antibodies, and DAPI (blue) to label the nucleus. The images show individual labeling and the fluorescence signals merged. Arrows indicate the regions with accumulation of cyclophilins and p47^{phox} in the cells. Bars = 5 μm. (C) Representative images are confocal immunofluorescence staining using the anti-p47-phox (green), super-resolution anti-HA antibodies (red). The merge images show individual labeling and the fluorescence signals merged (Yellow). The square indicates the zoom region. Bar = 1 μm.

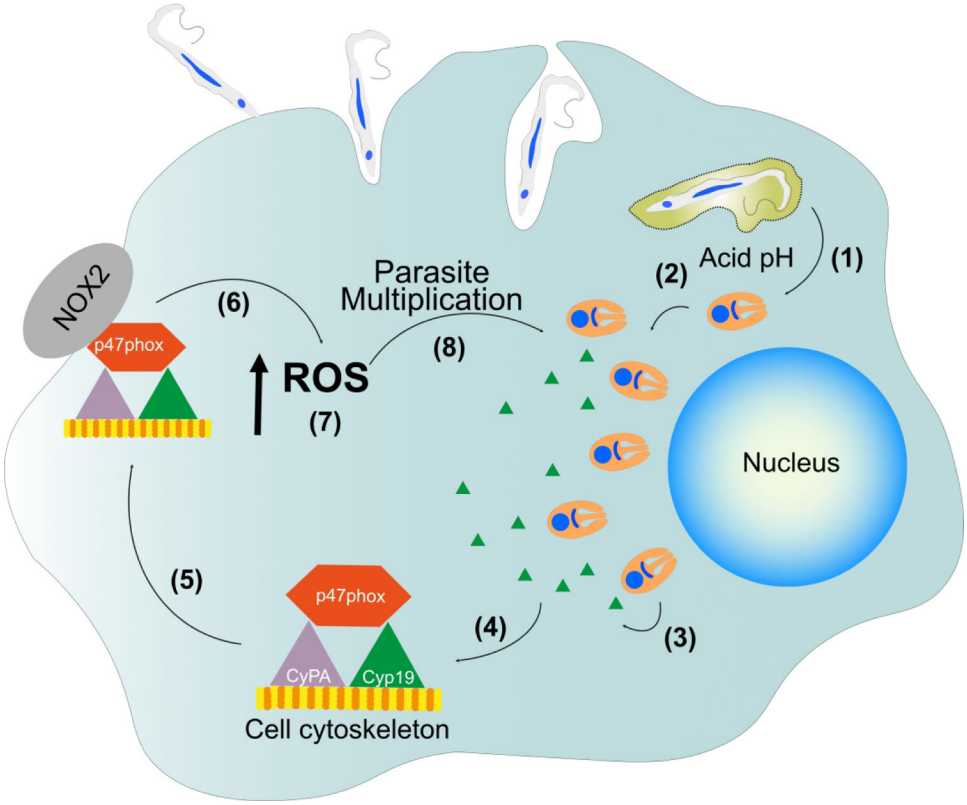

Figure 10 - Illustration of the proposed *Tc*Cyp19 role during *T. cruzi* infection.

After *T. cruzi* exits by acidification of the parasitophorous vacuole (1), and intracellular amastigotes start to proliferate (2) and secrete *Tc*Cyp19 into the host cell cytosol (3). *Tc*Cyp*19* interacts with the actin filaments (4) and carry the $p47^{phox}$ subunit to the cell edges (5). The complex forms at the leading edge of the cell and induces the activation of the NOX2-enzyme (6), leading to increased producing of anion superoxide and consequently increased ROS production (7), which enhances late amastigote multiplication (8).